Multivalent Afadin Interaction Promotes IDR-Mediated Condensate Formation and Junctional Separation of Epithelial Cells

Shuhei Kuno [1, #], Ryu Nakamura [2], Tetsuhisa Otani [3,4], and Hideru Togashi [1,4,5,*]

[1] Division of Molecular and Cellular Biology, Department of Biochemistry and Molecular Biology, Kobe University Graduate School of Medicine, Kobe 650-0017, Japan.

[2] Designing Department, Technology Solution Sector, Healthcare Business Unit, NIKON CORPORATION, Yokohama 244-8533, Japan

[3] Laboratory for Cell Biology and Biochemistry, Department of Biological Sciences, Graduate School of Science, Tokyo Metropolitan University, Hachioji, Tokyo 192-0397, Japan

[4] PRESTO, Japan Science and Technology Agency, Kawaguchi, Japan

[5] Laboratory of Molecular Pharmacology, Biosignal Research Center, Kobe University, Kobe 657-8501, Japan

[#] Division of Structural Medicine and Anatomy, Department of Physiology and Cell Biology Kobe University Graduate School of Medicine, Kobe 650-0017, Japan

* Correspondence: htogashi@people.kobe-u.ac.jp

[#] Present address

Summary

In epithelial cells, cell-cell adhesion is mediated by the apical junctional complex (AJC), which consists of tight junctions (TJs) and adherens junctions (AJs) aligned from the apical to the basal axis. However, the mechanism of AJC formation on the apical side and the separation of these junctions within AJCs are poorly understood. We found that multivalent interactions of afadin with adhesion molecules and the cytoskeleton lead to condensate formation in an intrinsically disordered region (IDR)-dependent manner, which promotes efficient accumulation in the linear AJ during initial junction formation. Furthermore, we found that endogenous afadin and ZO-1 were able to induce different condensate formations in the cell and that these condensates were segregated from each other. These properties of afadin explain how it strictly localizes to AJs in epithelial cells and is involved in regulating the segregation of AJ and TJ within the AJC.

Keywords, epithelial cells, cell-cell adhesion, initial junction formation, zonula adherens, afadin.

Introduction

Epithelial cells form sheets and tubes constituting most organs and tissues in animals, and cell-cell adhesion plays a vital role in epithelial cell morphogenesis and function. The primary mediator of cell-cell adhesion is the apical junctional complex (AJC), which comprises tight junctions (TJs) and adherens junctions (AJs) that are typically aligned from the apical to basal sides (Farquhar and Palade, 1963; Takeichi, 2014; Vogelmann and Nelson, 2005). In simple epithelia, cuboidal or columnar cells attach to each other through their lateral membranes. At the ultrastructural level, where the linear AJ is known as the zonula adherens (ZA) and is associated with a bundle of actin filaments, below the ZA, junctional structures extend to the basal ends of the cells, organizing the "lateral membrane contacts" (LCs) (Drenckhahn and Franz, 1986). Although LCs span the majority of junctions, they are linked to less-organized actin filaments (Nishimura et al., 2016). The mechanism by which the AJC forms on the apical side of the cell is not well understood, and the molecular mechanism by which TJs and AJs separate into apical and basal sides within the AJC remains unclear.

Previous studies have suggested that nectins initiate cell-cell adhesion and subsequently recruit the cadherin/catenin system to facilitate AJ formation (Takai and Nakanishi, 2003). Afadin, an anchoring protein that binds to nectin through the PDZ domain, localizes to AJs and interacts with various proteins, including cell adhesion molecules, signaling molecules, and the actin cytoskeleton (Huxham et al., 2021; Mandai et al., 2013). Afadin has two splicing isoforms, l-afadin and s-afadin. Epithelial cells mainly express l-afadin, which is the longest isoform that binds to nectin and F-actin (Mandai et al., 1997), here simply referred to as afadin. Afadin-knockout (KO) mice exhibit impaired AJ formation and apical-basal polarity, as well as TJs in the

neuroepithelium of the ectoderm, leading to embryonic lethality (Ikeda et al., 1999; Zhadanov et al., 1999). AJs are highly impaired in the ectoderm of afadin KO mice and embryoid bodies (Ikeda et al., 1999; Komura et al., 2008). Additionally, mice lacking afadin in nephron precursors fail to develop normal apical-basal polarity, leading to diminished integration of nectin complexes and failure to recruit cadherin (Yang et al., 2013). The phenotypes observed in afadin-KO mice suggest a crucial role of afadin in the formation of AJ and TJ. However, in cultured afadin-KO cells, there is evidence of cadherin-dependent cell adhesion and TJ formation, indicating phenotypic inconsistency with afadin-KO mice (Otani et al., 2019; Sakakibara et al., 2020). Canoe, the *Drosophila* homologue of afadin, was similarly identified as a component of AJ. A previous study showed that canoe is not essential for AJ assembly; however, its morphogenesis is impaired (Yang et al., 2013). Although our understanding of the molecular interactions involving afadin and canoe has advanced, there is still a gap in our understanding of how afadin functions in AJ formation.

Afadin and nectins are strictly localized to AJs in epithelial cells, whereas cadherin/catenin complexes are distributed widely along LCs (Mandai et al., 1997). During the initial phases of junction formation and epithelial polarization, nectin/afadin and cadherin/catenin complexes localize to primordial AJs; however, their localization cannot be distinguished. Localization of nectin/afadin and cadherin/catenin complexes differs with epithelial polarity establishment[6]. However, the mechanism by which the nectin/afadin complex strictly localizes to the proper location of AJ in epithelial cells remains unknown. Recently, it has been reported that cells and tissues utilize a known domain-independent protein-autonomous assembly mechanism called liquid-liquid phase separation to maintain function, and the intrinsically disordered region (IDR)-

dependent phase separation of ZO proteins drives TJ formation (Beutel et al., 2019; Kinoshita et al., 2022; Schwayer et al., 2019). Despite having a long C-terminal IDR, as suggested by protein sequence predictions for canoe and afadin (Gurley et al., 2023; Sun et al., 2022), afadin is not predicted to be a phase-separating protein (Rouaud et al., 2020). However, Gurley et al. recently reported severe morphological defects in head involution and dorsal closure in canoe mutants (Gurley et al., 2023). The severe phenotypes of the mutants were due to the loss of IDR, strongly suggesting the importance of an evolutionarily conserved IDR of canoe and afadin. This recent progress led us to hypothesize that IDR may play a role in the formation of AJ. In this study, we investigated the role of the C-terminal IDR of afadin during initial junction formation.

Results

Impairment of apical junction formation by loss of afadin

To investigate the role of afadin in the initial junction formation process in epithelial cells, we generated afadin-KO MDCK II (MDCK) cells, which possess typical epithelial junctions comprising AJCs and LCs. Successful KO was confirmed by western blotting (Otani et al., 2019) **(Fig. S1B)**. Initially, we examined the localization pattern of afadin, α-catenin, and F-actin through immunofluorescence staining in wild-type (WT) cells 24 h following replating. Afadin signals were observed along the apical junctions, but hardly on the LCs **(Fig. 1A)**. F-actin exhibited prominent localization along the apical edges of the junctions in a linear cable fashion and displayed an amorphous pattern in the LCs **(Fig. 1A, Boxed regions)**. α-catenin signals primarily localized at the apical junctions and were also detected at LCs **(Fig. 1A)**. Signals for α-catenin and F-actin colocalized at apical junctions and LCs. In afadin-KO cells, the linear signals of α-catenin and F-actin at apical junctions were markedly reduced, while the areal signals on the lateral side were notably increased **(Fig. 1A, X-Z)**. These observations were confirmed by densitometric analysis **(Fig. 1A, graph)**. Loss of linear localization of α-catenin and F-actin at the apical junctions indicated an impairment in linear AJ formation due to afadin KO.

We also examined the localization of α- and β-catenins in WT and afadin-KO cells 24 h following replating. These catenins fully colocalized, respectively **(Fig. 1B)**. Simultaneously, the tilt extent of LCs significantly increased in afadin-KO cells, accompanied by a reduction in cell height **(Fig. 1A,C)**. Despite these changes, the localization of the TJ-associated proteins, ZO-1 and Par-3, appeared nearly normal, with

a sharp line along the apical edges. These observations suggested that TJ formation was minimally affected by afadin KO **(Fig. 1D)**. These results support the notion that afadin regulates the localization of linear AJs but does not affect TJ formation in cultured MDCK cells.

Requirement of C-terminal IDR to apical localization of afadin

Afadin has multiple domains and is predicted to contain unique and extended IDRs in its C-terminal region (Gurley et al., 2023; Piovesan et al., 2018). To understand how afadin regulates apical junction formation in the epithelial cells, we conducted a domain analysis of afadin. Initially, we examined the junctional localization of EGFP-tagged afadin (EGFP-afadin) in afadin-KO cells **(Fig. 2A&S1A,C)**. EGFP-afadin was localized linearly along the apical junctions, fully restoring the localization of α-catenin and F-actin. We stably expressed various EGFP-afadin fragments in afadin-KO cells to understand the role of each domain in afadin localization. EGFP-afadinΔRA, EGFP-afadinΔPDZ, EGFP-afadinΔPR1-2, EGFP-afadinΔCC, and EGFP-s-afadin all localized linearly to apical junctions, similar to EGFP-afadin **(Fig. S1A,D)**. These results indicate that the function of a single domain cannot explain the apical localization of afadin.

Next, we investigated the effect of the IDR-containing C-terminal region of afadin on its localization. We generated EGFP-afadinΔC, truncated of the IDR-containing C-terminal region but retaining the F-actin binding region, and stably expressed it in afadin-KO cells **(Fig. S1C)**. These afadin fragments and full-length afadin were stably introduced into afadin-KO cells. Low expression clones were selected by FACS and confirmed by western blotting to be at levels comparable to endogenous levels **(Fig. S1C)**. Twenty-four hours after replating, most of the junctions of the EGFP-afadin-

expressing cells were linear and formed on the apical side. Immunofluorescence revealed that α-catenin and F-actin colocalized with apical linear junctions as in WT MDCK cells **(Fig. 2A)**. However, EGFP-afadinΔC did not localize apically but was diffusely distributed in the LCs. α-catenin and F-actin also diffusely localized on LCs, but did not accumulate in apical linear junctions, in a manner similar to afadinΔC. Furthermore, lateral contact area reduction was not observed in EGFP-afadinΔC-expressing cells **(Fig. 2A)**.

To further investigate the role of the C-terminal IDR of afadin in the localization of epithelial cells, we cultured the transfectants in collagen gel to allow for their growth into spherical cysts. Control EGFP-afadin-expressing cells formed typical epithelial cysts in which cells were arranged radially, and almost all EGFP-afadin localized at the apical junctions **(Fig. 2B)**. In contrast, although EGFP-afadinΔC-expressing cells formed single-lumen cysts, EGFP-afadinΔC failed to concentrate at the apical junction, the cells comprising the cysts were flattened, and these cell-cell junctions were tilted rather than radial **(Fig. 2B&S2A)**. The cell morphologies and structures of cell-cell junctions were remarkably similar to the results of the 2D culture. These results further confirm that the C-terminal IDR of afadin is important for apical localization and regulation of junction morphology.

Since nectins interact with afadin through their PDZ domain during AJ formation (Tachibana et al., 2000; Takahashi et al., 1999), we examined whether forced expression of nectin alters afadin localization to the apical junctions. Nectin-1 and EGFP-afadin or EGFP-afadinΔC were stably expressed in afadin-KO cells **(Fig. 2C)**. Afadin and exogenous nectin-1 in EGFP-afadin expressing cells colocalized along apical

junctions, hardly detected on LCs, with F-actin and α-catenin localized linearly along apical junctions **(Fig. 2C)**. In EGFP-afadinΔC-expressing cells, apical localization of afadin and nectin-1 was absent, and the linear signals of α-catenin and F-actin on apical junctions were not recovered. These findings indicate that nectin binding to afadin alone is insufficient for apical junctional localization of afadin.

Destabilization of apical accumulation by lack of C-terminal IDR of afadin

To further analyze the role of the C-terminal disordered region of afadin during initial junction formation, we conducted live imaging of cells expressing EGFP-afadin and EGFP-afadinΔC **(Fig. 3A&Video S1, S2)**. In the subconfluent cell layers, adherent cells extend and increase LC-like cell-cell contact. Live imaging showed that EGFP-afadin-expressing cells displayed convergence of cell-cell contacts to apical linear junctions, with EGFP-afadin concentrated linearly at the apical edge. In contrast, EGFP-afadinΔC signals were diffusely observed at LCs, displaying dynamic morphology changes but failing to form linear cell junctions within the observed timeframe **(Fig. 3A&Video S2)**. These results indicate that the C-terminal IDR of afadin is crucial for the convergence of cell-cell junctions from apical linear junctions. We also examined the effect of forced expression of nectin-1 in the accumulation of afadin in apical junction by live imaging and confirmed that EGFP-afadinΔC failed to accumulate at apical junctions even in the presence of nectin-1 **(Fig. 3B&Video S4)**.

Afadin regulates proper actomyosin association with AJs (Choi et al., 2016; Sakakibara et al., 2020; Sawyer et al., 2009). Therefore, we investigated whether myosin-induced contraction was involved in the apical accumulation of afadin during the initial junction formation. When the cells were treated with Y-27632 from the

beginning of culture (Uehata et al., 1997), afadin localized normally on the apical junctional complex within 24 h, indicating that myosin-dependent contractility was not involved in the apical accumulation of afadin during initial junction formation.

No requirement of interaction with α-catenin or ZO-1 in apical localization of afadin

Previous studies have shown that the region deleted in afadinΔC contains the PR1-2 region and the CC domain necessary for binding to ZO-1 or α-catenin (Maruo et al., 2018; Ooshio et al., 2010). To confirm the binding of afadin to ZO-1 or α-catenin, we immunoprecipitated each EGFP-afadin fragment from the lysates of HEK293 transfectants and analyzed the co-precipitated proteins by western blotting, confirming that the PR1-2 region and CC domains of afadin were required for binding to ZO-1 and α-catenin, respectively **(Fig. S1E,F)**. Then, we examined the apical accumulation of EGFP-afadinΔC+CC in afadin-KO cells to investigate whether the CC domain of afadin is required for its apical junctional localization. EGFP-afadinΔC+CC partially localized to the apical junctions, and extensive lateral contact sites remained **(Fig. S2B)**. The F-actin organization of EGFP-afadinΔC+CC-expressing cells was similar to that of afadin-KO cells **(Fig. S2B)**. Live imaging showed that EGFP-afadinΔCC, EGFP-afadinΔPR1-2, but not EGFP-afadinΔC+CC accumulated in the apical junctions during initial junction formation **(Fig. S3A&Video S5, S6, S7)**. These observations also suggest that the PR1-2 region and CC domain of afadin, which bind to ZO-1/2 and α-catenin, are not required for the apical localization of afadin.

To determine whether ZO-1/2 or αE-catenin is necessary for the apical localization of afadin, we examined its localization in ZO-1/2 double KO (dKO) cells and αE-catenin KO MDCK cells, which were previously generated **(Fig. S1G,H)**[14]. To assess the junctional localization of afadin, αE-catenin, and ZO-1 in ZO-1/2 dKO and αE-catenin KO cells, the cells were triple-stained with antibodies 24 h after replating **(Fig. S2D,E)**. In ZO-1/2 dKO cells, afadin and α-catenin were apically localized but exhibited a somewhat broad distribution in apical junctions **(Fig. S2D)**. In αE-catenin KO cells, despite unstable intercellular adhesions and reduced accumulation of afadin at cell-cell contacts, afadin and ZO-1 were colocalized at the apical side where cell-cell contacts formation was observed **(Fig. S2E, X-Z)**. These observations suggest that ZO-1/2 and α-catenin are not responsible for the apical localization of afadin, although these molecules may be involved in the strict localization of afadin in AJCs.

For a detailed analysis of the molecular behaviors of afadin and afadinΔC in ZO-1/2 dKO and αE-catenin-KO cells during initial junction formation, live imaging was conducted **(Fig. S3B,C&Video S8, S9, S10, S11)**. EGFP-afadin-expressing ZO-1/2 dKO cells exhibited the convergence of spreading LCs to apical linear junctions, with EGFP-afadin concentrated linearly at the apical edge. In contrast, EGFP-afadinΔC-expressing ZO-1/2 dKO cells displayed diffuse signals at LCs, which failed to converge to linear cell junctions **(Fig. S3B)**. Live imaging of αE-catenin-KO cells revealed the accumulation of EGFP-afadin at the apical junctions. However, in EGFP-afadinΔC-expressing cells, partial linear localization of EGFP-afadinΔC signals and vigorously moving lateral contact sites were observed **(Fig. S3C&Video S10, S11)**. These results

suggest that ZO-1/2 or αE-catenin is not required for apical convergence of afadin from LCs.

Implication of C-terminal IDR of afadin in condensates formation.

Our observations suggest that the C-terminal region of afadin plays a role in the accumulation of apical junctions during initial junction formation, independent of its known binding partners. As mentioned previously, the C-terminal region of afadin is predicted to contain IDRs **(Fig. S4A)**. Increasing evidence suggests that multivalent protein-protein interactions mediated by IDRs facilitate the formation of condensates[30]. We transiently expressed EGFP-afadin in HEK293 cells to assess whether afadin forms IDR-dependent condensates. High EGFP-afadin expression resulted in the formation of large condensates **(Fig. 4A)**. These dynamic condensates fused within seconds, indicating liquid-like properties **(Fig. S4B&Video S12)**. We then transiently expressed various EGFP-afadin fragments in HEK293 cells to understand the role of each domain in condensate formation. EGFP-afadinΔRA, EGFP-afadinΔPDZ, EGFP-afadinΔPR1-2, EGFP-afadinΔCC, and EGFP-s-afadin all form condensates in the cells, similar to EGFP-afadin **(Fig. 4A)**. However, in EGFP-AF_N-PDZ- or EGFP-afadinΔC-expressing cells, the EGFP signal was higher in the cytoplasm, and condensate formation was significantly reduced compared to cells expressing EGFP-afadin **(Fig. 4A)**. Although higher expression induced the formation of large condensates, these observations suggested that afadin inherently possesses the capacity to form condensed compartments in an IDR-dependent manner in cells. Upon comparison of the results shown in Fig.4A and Fig. S1D, the localization of afadin to apical AJs was found to correspond to its

ability to form condensates, suggesting that IDR-dependent condensate formation of afadin might be involved in the regulation of its localization.

To investigate the mechanism regulating afadin condensate formation in HEK293 cells, we treated the cells with 1,6-hexanediol (HD). Aliphatic alcohol 1,6-HD has been widely used to study the formation process of membrane-less condensates; 1,6-HD inhibits weak hydrophobic protein–protein interactions required for the formation of liquid-like condensates (Itoh et al., 2021; Lin et al., 2016). Since ZO-1 has been reported to form condensates induced by overexpression (Beutel et al., 2019; Kinoshita et al., 2022; Schwayer et al., 2019), we used ZO-1-EGFP as a control. Treatment with 1,6-HD of cells expressing EGFP, EGFP-afadin, and ZO-1-EGFP showed that 5% and 10% 1,6-HD reduced the condensates of afadin and ZO-1 within 5 min in a concentration-dependent manner, suggesting that weak hydrophobic protein–protein interactions formed these condensates in the cells **(Fig. 4B)**. Subsequently, we constructed the EGFP-AF_1114-1654 fragment, containing only the IDR region deleted in afadinΔC **(Fig. S4A)**, and transiently expressed EGFP-AF_1114-1654 in HEK293 cells **(Fig. 4C)**. EGFP-AF_1114-1654 expression resulted in the formation of abundant condensates **(Fig. 4C)**. These results support the idea that the C-terminal IDR of afadin is required for hydrophobic protein-protein interactions to form condensates.

To determine whether ZO proteins were required for afadin to form condensates, we transiently expressed EGFP-afadin in ZO-1/2 dKO MDCK cells. Previous studies have shown that exogenous afadin is enriched in the condensed ZO-1 phase of HEK293 cells (Beutel et al., 2019). We observed the formation of EGFP-afadin condensates in ZO-1/2 dKO cells **(Fig. S4C)**. These results indicated that EGFP-afadin condensates were formed in a ZO-independent manner.

Liquid like condensate formation of junctional afadin.

To examine the impact of F-actin polymerization disassembly on the molecular behavior of afadin already localized at cell-cell junctions, we treated subconfluent afadin-KO MDCK cells expressing EGFP-afadin or EGFP-afadinΔC with latrunculin-B (LatB), which reversibly blocks actin polymerization. EGFP-afadin was initially linearly localized at the apical junctions; however, after 90 min of LatB treatment, continuous junctional afadin was segmented into a series of condensates **(Fig. 5A)**. However, the localization of afadinΔC was unaffected by LatB treatment, and no condensates were observed **(Fig. 5A)**. As a control, we examined the localization of αE-catenin-EGFP in αE-catenin-KO cells following LatB treatment. In αE-catenin-EGFP-expressing cells, some junctional αE-catenin-EGFP was partially fragmented from its linear localization 90 min following LatB treatment, but no condensates were observed. Live-cell imaging revealed that the formation of afadin condensates followed the fragmentation of junctional afadin, which actively moved and fused into condensates **(Fig. 5B&Video S13)**. However, in EGFP-afadinΔC-expressing cells, these behaviors were not observed, and junctional afadin remained stable following LatB treatment **(Fig. 5B&Video S14)**.

Next, to investigate the formation of condensates from junctional afadin, we examined the molecular behavior in a mixed culture of EGFP-afadin- and mScarlet-afadin-expressing afadin-KO MDCK cells **(Fig. 5C)**. In the heterotypic cell-cell junctions between EGFP-afadin- and mScarlet-afadin-expressing cells, EGFP-afadin, mScarlet-afadin, and F-actin colocalized, suggesting the normal formation of AJs between these cells. In contrast, in the presence of LatB for 90 min, these signals were observed in the condensates at cell junctions. Interestingly, the F-actin signal was

observed throughout the individual condensates, whereas the EGFP and mScarlet signals were symmetrical on both sides of the condensates. This result indicates that afadin, which forms condensates in individual cells, behaves as a dynamic condensate when linked between cells.

To understand the relationship between the molecular interactions and condensate formation of endogenous afadin and ZO-1, we examined the localization of afadin and ZO-1 in WT MDCK cells in the presence of LatB using immunofluorescence staining **(Fig. 5D)**. After 90 min of LatB treatment, endogenous afadin and ZO-1 were fragmented at the cell junctions and had a condensate-like morphology, consistent with the observations of afadin in Fig. 5A **(Fig. 5D)**. When 1,6-HD was added after LatB treatment to confirm whether these were condensates, we observed that these structures disappeared, whereas 2,6-HD did not yield the same results **(Fig. S5B)**. To examine the localization of afadin and ZO-1 in more detail, cell junctions were observed at a high magnification **(Fig. 5D, Right)**. The condensate-like structures of endogenous afadin and ZO-1 were adjacent to each other without colocalization, suggesting that these condensate-like structures are segregated in the juxta-membrane region. This suggests that the condensates of ZO-1, which are thought to act as the constitutive hubs of TJs, and those of afadin, function in different fractions. In summary, the results suggest that afadin condensates not only exhibit liquid-like properties in AJs but also function intercellularly in a manner that is distinct from the TJ phase-separated compositional function of ZO-1.

To confirm the endogenous expression level of afadin condensates, WT MDCK cells were cultured in the presence of 1,6-HD for 5 min, followed by localization observation using immunofluorescence for afadin, ZO-1, and α-catenin **(Fig. 5E)**. We

found that endogenous afadin localization disappeared from AJs, while ZO-1 and α-catenin still localized in the junctions in a linear fashion **(Fig. 5E)**. This result indicates that afadin lost its localization to AJs in a 1,6-HD-dependent manner. In contrast, ZO-1 and α-catenin did not lose their localization, suggesting that the apical localization of afadin is not dependent on its binding to ZO-1 or α-catenin.

Apical accumulation of chimeric afadin of FUS-derived IDR and afadinΔC

Our results indicate that the nature of IDRs causes the apical accumulation of afadin. If the localization of afadin is regulated by IDRs, it is conceivable that the IDRs of other molecules may also be responsible for its apical localization. Although several proteins are involved in IDR-dependent condensate formation, the RNA-binding protein Fused in Sarcoma (FUS) is one of the most studied proteins in terms of its liquid-liquid phase separation properties (LLPS) (Burke et al., 2015; Patel et al., 2015; Shimobayashi et al., 2021). The low-complexity N-terminal IDR of FUS (FUSn) is responsible for its structural disorder in solution and formation of a liquid-like phase-separated state. To test this idea, we constructed EGFP-afadinΔC+FUSn, which consists of an FUSn sequence added to the C-terminal side of the EGFP-afadinΔC fragment **(Fig. S6A, See also STAR methods)**. The IDR sequences in FUS have been shown to be involved in condensate formation (Shin et al., 2017). To confirm the properties of EGFP-afadinΔC+FUSn, we transiently expressed this fragment in HEK293 cells and observed condensate formation **(Fig. S6B)**. This indicated that FUSn was responsible for condensate formation. We then stably expressed EGFP-afadinΔC+FUSn fragments in afadin-KO cells to examine the effect of the FUSn sequence on afadinΔC localization.

EGFP-afadinΔC+FUSn localized linearly along the apical junctions, and the localization of LCs was drastically reduced **(Fig. 6A)**. The FUSn sequence is not known to interact with any cell adhesion-related molecule, and the addition of this sequence resulted in the apical localization of afadin, suggesting that IDRs are required for the accumulation of afadin at the apical junctions of cells.

Altered distribution of afadin within the AJC by different IDR

To obtain more detailed information about the distribution of EGFP-afadinΔC+FUSn, we immunostained cells expressing EGFP-afadin and EGFP-afadinΔC+FUSn with ZO-1 and β-catenin and observed the cells using super-resolution confocal microscopy. EGFP-afadin colocalized with β-catenin and ZO-1 at the AJCs, and these molecules appeared to be closely associated without apparent separation. Although EGFP-afadinΔC+FUSn was also localized to the AJCs, its distribution differed from that of EGFP-afadin; the localization of EGFP-afadinΔC+FUSn was shifted away from the ZO-1 and β-catenin in both X-Y and X-Z planes **(Fig. 6B,C)**. The distribution of these molecules was assessed by line scan, which revealed a minimal shift in localization between ZO-1 and β-catenin for EGFP-afadin, contrasting with a substantial shift observed for EGFP-afadinΔC+FUSn **(Fig. 6C)**. Furthermore, a reduced frequency of colocalization was observed with ZO-1 and β-catenin, and the colocalized regions of these molecules were significantly reduced **(Fig. 6C)**. These observations indicate that the FUS-derived IDR added to afadinΔC allows it to localize apically **(Fig. 6B, X-Z)**. However, the distinct distribution of EGFP-afadinΔC+FUSn compared to EGFP-afadin

suggests that the different IDRs may have resulted in a different distribution within the AJC.

As shown in Fig.5D, endogenous afadin and ZO-1 formed different condensates in the cells, suggesting that these condensates did not mix. Furthermore, because differences in the IDR regions cause differences in the localization of afadin in Fig.6B, we considered the possibility that differences in IDRs regulate molecular localization within the AJC. To test this hypothesis, we constructed EGFP-afadinΔC+PSG, which consists of the PDZ1-SH3-GuK (PSG) sequence of ZO-1 on the C-terminal side of the EGFP-afadinΔC fragment **(Fig. S6A, See also STAR methods)** because the PSG domain of ZO-1 is known to localize to the initial AJ through dimerization between ZO-1[37]. To confirm the properties of EGFP-afadinΔC+PSG, we transiently expressed this fragment in HEK293cells and observed condensate formation **(Fig. S6B)**. We then stably expressed EGFP-afadinΔC+PSG in afadin-KO cells to examine their localization in the AJC. The localization of EGFP-afadinΔC+PSG was similar to that of EGFP-afadinΔC+FUSn, with linear localization to AJC, while there was little localization to the lateral contacts **(Fig. 6B)**. The distribution of EGFP-afadinΔC+PSG was quantified by a line scan, which revealed a significant peak shift in localization between ZO-1 and β-catenin compared to EGFP-afadin **(Fig. 6C)**. However, the localization of EGFP-afadinΔC+PSG was close to ZO-1 and far from β-catenin. Interestingly, EGFP-afadinΔC+PSG and ZO-1 were separated from each other and localized in a double-linear manner within the apical junction complex **(Fig. 6B)**. These observations suggest that differences in the nature of IDRs regulate their distribution within the AJC in epithelial cells **(Fig. 6D)**.

Discussion

Correct positioning of the AJ is considered a crucial step in establishing apical-basal polarity and TJ formation in epithelial cells. Afadin and nectins are strictly localized to AJs in epithelial cells; however, the mechanism underlying this localization remains unknown. Afadin-KO mice exhibit impaired AJ formation, disruption of apical-basal polarity, and TJ formation in the neuroepithelium of the ectoderm (Ikeda et al., 1999; Zhadanov et al., 1999). The abnormalities observed in afadin-KO mice are likely attributable to the failure of AJs to form in their proper positions. Despite its recognized importance, the precise mechanisms by which afadin regulates intercellular adhesion and polarity remain elusive. The present study revealed that afadin accumulates at the apical junction of cells, driven by the nature of its IDRs, independent of known domains during initial junction formation. Deletion of the afadin IDR suppressed its apical accumulation and concomitantly reduced the accumulation of the cadherin/catenin complex and F-actin. When the IDR fragment of afadin was overexpressed in cells, it formed condensates; however, IDR alone did not accumulate at the apical junction **(Fig. S4D)**. Intriguingly, replacing the IDR of afadin with the IDR of FUS restored apical localization but altered the distribution of afadin within the AJC. These results indicate that IDR is necessary not only for apical localization but also for regulating their distribution within the AJC. The IDR at the C-terminus of afadin alone is not sufficient for junctional localization, and the N-terminus of afadin without the IDR cannot successfully converge to the apical junctions. When afadin accumulates in apical AJs, multivalent interactions through the adhesion molecules and the cytoskeleton may trigger IDR-mediated condensate formation, which may facilitate efficient accumulation.

IDR-dependent apical localization of afadin

Takai et al. reported that nectin and cadherin are diffusely distributed on the free surface of the membranes of migrating cells at the initial stage of AJ formation. When two migrating cells contact each other through protrusions such as filopodia and lamellipodia, nectin first forms trans-dimers at intercellular contact sites, and nectin/afadin complexes recruit cadherin to the initial contact sites. Subsequently, nectin/afadin gradually localizes towards the apical side, resulting in the linear localization of the actin cytoskeleton and cadherin/catenin complexes at the apical side, eventually developing into more mature AJs (Takai et al., 2008). Our study revealed that apical localization of afadin, mediated by IDRs, triggers the formation of linear junctions on the apical side of epithelial cells. Interestingly, the PDZ domain of afadin was not essential for apical localization, suggesting that nectins do not determine the localization of afadin; rather, afadin define AJ localization of nectins. Moreover, EGFP-afadinΔC+FUSn, in which the IDR of afadin was replaced with an FUS-derived IDR, was also localized to the apical AJ, but its distribution within the AJC was different. These results indicate that the IDR is responsible for the distribution of afadin within the AJC.

How does afadin localize to the apical AJ. Noordstra et al. recently reported that antiparallel cortical flows at nascent AJs exert tension on the α-catenin actin-binding domain, causing it to increase adhesion growth (Noordstra et al., 2023). This retrograde flow may be involved in the apical accumulation of afadin. Cadherin flow is also known as the cytoskeleton-dependent movement of the adhesive surface, which is a flow-like movement of cadherin molecules from the basal to the apical direction at the cell junction and is associated with the reorganization of actin filaments. However, afadin localizes to apical junctions even when myosin-dependent junctional contraction is inhibited,

suggesting that the mechanism of apical afadin accumulation differs from that of cadherin flow **(Fig. 3C)**. Moreover, EGFP-AF_C, which is a fragment of the IDR of afadin with an F-actin-binding (FAB) domain, rarely localizes to apical junctions **(Fig. S4A, D)**. These findings suggest that neither myosin-mediated contractility nor actin cytoskeleton binding alone is sufficient for the apical localization of afadin.

We demonstrated that EGFP-afadin ΔC failed to localize to the apical junctions, whereas the chimeric molecule EGFP-afadinΔC-FUSn, in which the IDRs of the RNA-binding protein FUS sequence were added to EGFP-afadin ΔC, exhibited a linear localization along the apical junctions **(Fig. 6A)**. Since the EGFP-afadinΔC-FUSn sequences lack the domains for interactions with α-catenin or ZO-1, it is likely that the localization of afadin to the apical junctions is not regulated by its direct interactions with these molecules.

How do IDRs of afadin accumulate at apical junctions? Afadin and canoe are also known for their roles in spindle orientation and apical-basal positioning of the lumen (Wee et al., 2011). Keder et al. reported that phosphorylation of specific amino acids near the start of the C-terminal IDR of the canoe is important for apical localization in neuroblast cells (Keder et al., 2015). This sequence is conserved in the PR1-2 region of the mammalian afadin. However, our observation that afadin, which does not contain the PR1-2 region, localizes to apical junctions suggests that different mechanisms may be involved in the regulation of apical localization in mammalian epithelial cells than in *Drosophila* neuroblast cells. In addition, afadin and canoe contain an RA domain, which interacts with Rap1 GTPase and regulates AJ positioning in *Drosophila* (Bonello et al., 2018). During canoe apical localization, Rap1 and actin-dependent mechanisms are implicated (Sawyer et al., 2009). The regulation of the apical localization of afadin by

Rap1 was also examined in MDCK cells, revealing that afadin ΔRA mutants, which are unable to bind Rap1, increase apical localization (Hoshino et al., 2005). Although it is clear that Rap1 is involved in the apical localization of canoe and afadin, the detailed mechanisms require further investigation. Since actin filaments are involved in AJ formation and contribute to polarity formation by directional elongation, the direct or indirect interaction between afadin and actin may be responsible for the accumulation at the apical side. In addition, nectin-dependent initial adhesion may promote and stabilize this interaction.

IDR-dependent molecular segregation between afadin and ZO-1

In the present study, we showed that condensates of endogenous afadin and ZO-1 segregated in the juxtamembrane region in Fig.5D. This suggests that molecular segregation between afadin and ZO-1 is possibly involved in the sorting of two distinct junctional domains during epithelial polarization. In afadin-KO cells, no abnormalities were observed in the localization of ZO-1 and Par-3, and the epithelial barrier function was not affected (Otani et al., 2019). This suggests that the regulation of AJ and TJ formation may be independent, at least in cultured epithelial cells. Previous studies have shown that ZO-1/2 is essential for TJ formation (Otani et al., 2019; Umeda et al., 2006); however, ZO-1/2 was not essential for the apical localization of afadin **(Fig. S2D)**. Furthermore, since afadin KO had no significant effect on TJ formation in the cultured cells, but had a notable effect on AJ formation, ZO-1 could be considered the organizer of TJ and afadin can be considered the organizer of AJ. Mangeol et al. recently showed that ZA consists of two distinct belts of adhesive complexes, an apical one with nectin/afadin and a basal one with cadherin/catenin (Mangeol et al., 2024). The structural

segregation of TJ and AJ within the AJC is likely caused by the autonomous separation of afadin and ZO-1. The layered structure within the linear AJ may be formed by the autonomous condensate-formation ability of afadin, which is the driving force behind its separation from cadherin/catenin complexes.

Materials and methods

Cell culture

MDCK-II (Richardson et al., 1981) and HEK293 (Graham et al., 1977) cells were grown in a Dulbecco's Modified Eagle Medium: Nutrient Mixture F-12 Ham (#11574546, Gibco) supplemented with 10% fetal bovine serum (FBS) (#2917254, MP Biomedicals) (DH10) at 37°C with 5% CO_2, these cells were kindly gifted by Dr. Masatoshi Takeichi (RIKEN Center for Biosystems Dynamics Research, Kobe, Japan). Generation of afadin KO, ZO-1/2 dKO, and αE-catenin KO MDCK cells was previously described [14].

Three-dimensional Cell culture

For three-dimensional (3D) culture, MDCK cells were embedded in bovine dermis atelocollagen gel (#IPC-50; Koken). Briefly, atelocollagen gel and cell suspension prepared in DH10 and 20 mM HEPES (pH 7.5) (#15630080, Gibco) were mixed at a 4:6 ratio on ice, and 200 μl with 4.5×10^4 cells in the medium was plated on 13-mm-diameter cover glass (#3460, Matsunami Glass) in 24-well plate (#142475, Nunc) or 35-mm-diameter glass bottom dishes (#D11530H, Matsunami Glass). The gel was allowed to form at 37°C under 5% CO_2 for 30 minutes, and 500 μl of warm DH10 was added

into the plate or dish.

Expression vectors

The following expression vectors were used, pCANw-sal-EGFP, pCAH, and pCAB (Ichii and Takeichi, 2007), and the following vectors were modified from the aforementioned vectors, pCANw-EGFP-C3, pCANw-mScarlet-C3, and pCANw-sal-mScarlet. mScarlet cDNA (without SalI, NotI, AhdI and SacII restrict enzymic sites) was synthesized at Genewiz (Bindels et al., 2017). The following afadin mutants and chimeras were used by PCR amplification and Gibson assembly: The full-length cDNA for rat afadin (amino acids 1-1828) and cDNAs for afadinΔRA (amino acids 351-1828 (Hoshino et al., 2005)), afadinΔPDZ (amino acids 1-1015 and 1122-1828 (Nakata et al., 2007)), afadinΔC (amino acids 1-1113 and 1655-1828), afadinΔPR1-2 (amino acids 1-1218 and 1400-1828 (Ooshio et al., 2010)), afadinΔCC (amino acids 1-1399 and 1461-1828 (Maruo et al., 2018)), s-afadin (Kobayashi et al., 2014), AF_1114-1654 (amino acids 1114-1654), afadinΔC+CC (amino acids 1-1113, 1400-1466, and 1655-1828), afadinΔC+FUSn (amino acids 1-1113, human FUS_1-214 (Shin et al., 2017), and 1655-1828) and afadinΔC+PSG (amino acids 1-1113, mouse ZO-1_PSG (Beutel et al., 2019), and 1655-1828). Afadin cDNAs were also subcloned into pCANw-EGFP-C3, pCANw-

mScarlet-C3, pCAH-EGFP-C3, and pCAH-mScarlet-C3 using KOD One PCR Master Mix (#KMM-101X5, TOYOBO) and NEBuilder HiFi DNA Assembly Master Mix (#E2621L, New England Biolabs), according to the manufacturer's instructions. Mouse αE-catenin cDNA (Katsunuma et al., 2016) was subcloned into pCANw-sal-EGFP and pCANw-sal-mScarlet by digestion and ligation. pCA-ZO-1-HA, pCAH-ZO-1-EGFP, pCANw-ZO-1-EGFP, and pCAH-nectin-1 were previously described (Matsuda et al., 2004; Otani et al., 2006; Otani et al., 2019; Togashi et al., 2011). See also resource tables.

DNA transfection

HEK293 cells were transfected with various combinations of expression vectors in 10-cm dishes. Transfection were performed with PEI MAX (#24765-1, Polysciences) or Lipofectamine 3000 (#L3000075, Invitrogen), according to the manufacturer's instructions. Afadin KO, αE-catenin KO and ZO-1/2 dKO MDCK cells were transfected with expression vectors, respectively. Transfection of expression vectors was performed with Lipofectamine 3000, according to the manufacturer's instruction.

Generation of stable transfectants.

The transfected MDCK cells were selected using 400 μg/ml G418 disulfate (#08973-14,

NacalaiTesque) or 200 μg/ml hygromycin B Gold (#ant-hg-2, Invivogen), the mixed clones with the lowest EGFP expression were collected by a FACS (SH800Z, SONY). These multiple clones were maintained in the presence of G418 disulfate or hygromycin Gold B.

Antibodies and Reagents

The following primary antibodies (Ab) were used: anti-afadin mouse monoclonal Ab (mAb) (#AM26175PU-N, clone 3, OriGene; 1:50 dilution for immunofluorescence, 1:3000 dilution for western blotting[55]), anti-α-catenin rabbit polyclonal Ab (pAb) (#C2081, Sigma-Aldrich; 1:400 dilution for immunofluorescence, 1:1000 dilution for western blotting), anti-Par-3 rabbit pAb (#07-330, Sigma-Aldrich; 1:100 dilution for immunofluorescence), anti-β-catenin mouse mAb (#MAB2081, clone 5H10 (Johnson et al., 1993), Sigma-Aldrich; 1:1000 dilution for immunofluorescence), anti-β-catenin rabbit pAb (#C2206, Sigma-Aldrich; 1:800 for immunofluorescence), anti-ZO-1 rat mAb (#sc-33725, clone R40.76 (Anderson et al., 1988), Santa Cruz Biotechnology; 1:50 dilution for immunofluorescence, 1:1000 dilution for western blotting), anti-HA rat mAb (#11867431001, clone 3F10, Roche; 1:4000 dilution for western blotting), anti-α-tubulin mouse mAb (#T6199, clone DM1A (Blose et al., 1984), Sigma-Aldrich, 1:5000

dilution for western blotting), anti-GFP rat mAb (#04404-84, clone GF090R, NacalaiTesque; 2.5 μg/reaction for co-immunoprecipitation).

For immunofluorescence, primary Abs were visualized with secondary goat antibodies conjugated with Alexa Fluor plus 405, Alexa Fluor 488, Alexa Fluor 647 (#A48255, #A-11008, #A-11001, #A-21245, Invitrogen; #115-605-146, Jackson Immunoresearch Laboratories; 1:400 dilution), and Cy3 (#AP136C, Sigma-Aldrich; 1:400 dilution).

For nuclei and F-actin staining were visualized with 4',6-diamidino-2-phenylindole (DAPI) (#D523, Dojindo; 1:1000 dilution) and phalloidin Alexa Fluor plus 405-conjugated (#A30104, Invitrogen; 1:400 dilution), phalloidin ATTO 565-conjugated (#94072, Sigma-Aldrich; 1:200 dilution), and phalloidin Alexa Fluor 647-conjugated (#A22287, Invitrogen, 1:100 dilution). For western blotting, primary Abs were detected with secondary rabbit, mouse, and rat pAbs horseradish peroxidase-conjugated (HRP-Ab) (#111-035-003, #115-035-003, Jackson Immunoresearch Laboratories; #31470, Invitrogen; 1:5000 dilution).

The following inhibitors with dimethyl sulfoxide (DMSO) (#046-21981, FUJIFILM Wako Pure Chemical Corporation) were used: 1,6-hexanediol (1,6-HD) (#17913-72, NacalaiTesque), 2,5-hexanediol (2,5-HD) (#H11904-50G, Sigma-Aldrich)

Y-27632 (Uehata et al., 1997)(#253-00513, FUJIFILM Wako Pure Chemical Corporation), and latrunculin B (LatB) (#3974, Tocris Bioscience).

Immunofluorescence

Cultured cells for 24 hours of incubation were fixed with 4% paraformaldehyde (PFA) (#104005, Merck) in Hank's balanced salt solution containing 1 mM Ca^{2+} and Mg^{2+}, containing 10 mM HEPES (HBSS CM+) at 37°C for 15 minutes. After fixation, the samples were washed three times with Tris-buffered saline, pH 7.6 containing 1mM Ca^{2+} (TBS-C) and permeabilized with a 0.25% Triton X-100 in TBS-C at room temperature (RT) for 5 minutes. The samples were then blocked with 5% normal goat serum (#NS02L, Sigma-Aldrich) in TBS-C at RT for 30 minutes, followed by incubation with primary antibodies (Abs) in 2.5% normal goat serum in TBS-C or in "Can Get Signal" immunoreaction enhancer solution B (#NKB-601, TOYOBO) at RT for 2 hours. The samples were washed three times with TBS-C, then incubated with secondary Abs and counterstain dyes in 2.5% normal goat serum in TBS-C at RT for an hour. These samples were washed three times with TBS-C and mounted on a slide glass with CC/Mount (#K002, Diagnostic Biosystems).

3D culture cells for 8 days were incubated with collagenase type VII (#C0773;

Sigma-Aldrich) at RT for 15 minutes. The cells were fixed with 2% PFA in HBSS CM+ at 37°C for 30 minutes. After another two rinses with TBS-C, the cells were blocked with 0.5% Triton X-100 and 5% normal goat serum in TBS-C at RT for 30 minutes. The primary Abs were diluted in "Can Get Signal" immunoreaction enhancer solution B and incubated with the gels at 4°C overnight with gentle rocking. The gels were washed with TBS-C five times and incubated with the secondary Abs overnight at 4°C with gentle rocking. After five washes with TBS-C, the samples were mounted in CC/Mount. A tall sample was mounted into the bank of a microscope slide by hollowing out the inside of vinyl tape.

Images were obtained with confocal laser scanning microscopes (AX-R, Nikon Corporation; LSM700 and LSM900 with Airyscan 2, Carl Zeiss Microscopy; FV1000, OLYMPUS Life Science) equipped with a CFI Plan Apochromat Lambda D 60x/1.42 Oil (Nikon Corporation), a LD LCI Plan-Apochromat 40x/1.2 Imm (Carl Zeiss Microscopy), Plan-Apochromat 63x/1.4 Oil (Carl Zeiss Microscopy), a UPLSAPO 20x/0.75 (OLYMPUS Life Science), and a PLAPON60XOSC2 60x/1.4 (OLYMPUS Life Science) lens. These images were processed and analyzed with ZEN 3.9.1 software into "bioformat import" function (Carl Zeiss Microscopy). Line fluorescence intensities were scanned along arrows and normalized per 6 pixels using the "Profile View"

function. Cell height was measured using the "Ortho View" function of nuclei and β-catenin signals. Cell height of Cyst was measured using the β-catenin Z-projection signal. The tilting extent was measured as referenced in the previous report (Nishimura et al., 2016). The degree of tilting of LCs was quantified as follows: LC area was defined as EGFP-afadins or β-catenin signals. Then, the width of the border between the LC and AJC areas was measured. Subsequently, the LC area was divided by the width of the border to obtain a mean LC area per AJC unit (1 μm). This value was defined as the "tilting extent." Condensate number of the cell was measured by orthogonal projection images. Statistical tests and graphs were performed using Kyplot 6.0.2 software (Yoshioka, 2002).

Western blotting

The samples separated by SDS-PAGE were transferred to polyvinylidene difluoride membranes (#IPVH00010, Millipore). After the membranes were blocked with Block ACE (#UK-B80, KAC) in Tris-buffered saline, pH7.6 containing 0.05% Tween 20 (TBS-T), they were incubated with the indicated Abs at 4°C overnight. After the membranes were washed with TBS-T three times, they were incubated with HRP-Abs. The membranes were then washed with TBS-T three times, and signals for the proteins

were detected using Chemi-Lumi One L (#078800, NacalaiTesque) and a chemiluminescent image analyzer (LAS-4000, FUJIFILM Wako Pure Chemical Corporation).

Co-immunoprecipitation

The transfected HEK293 cells were washed with phosphate-buffered saline and then suspended in 1ml of Buffer A (20 mM Tris-HCl, pH 7.4, 150 mM NaCl, 1% Triton X-100, 1 mM EDTA, 1 mM Na_3VO_4, and protease inhibitor cocktail for use with mammalian cell and tissue extracts (#25955-11, NacalaiTesque) on ice. The cell extract was obtained by centrifugation at 15,000 rpm at 4°C for 15 minutes (MX-300, TOMY). Protein loadings were normalized by protein assay BCA kit (#06385-00, NacalaiTesque). 500 μg of cell extracts was then incubated with 2.5 μg of anti-GFP mAb at 4°C overnight. The reactants were incubated with dynabeads protein G slurry (#10004D, Invitrogen) at RT for an hour. After supernatant discard, the beads were extensively washed with Buffer A, and the bound proteins were eluted by boiling the beads in 55 μl of 6× SDS sample buffer (62.5 mM Tris-HCl, pH 6.8, 2% SDS, 0.1 M dithiothreitol, 10% glycerol, and 0.01% bromophenol blue) for 5 minutes. Each 10 μl of the samples were then subjected to SDS-PAGE, followed by western blotting with the anti-afadin, -HA, and -α-catenin.

1

2 **Live cell imaging**

3 Live imaging of MDCK cells was performed using a confocal laser scanning microscope
4 (FV1000, OLYMPUS Life Science) equipped with a standard heating stage top
5 incubator (INUB-ZILCS, TOKAI HIT) at 37°C under 5% CO_2. The cells were seeded
6 onto a 35-mm-diameter glass bottom dish (#D11530H, Matsunami Glass) and observed
7 with a UPLSAPO30XS, or a PLAPON60XOSC2 lens. Before experiments, the cell
8 media were replaced with 3 ml of FluoroBrite DMEM (#A1896702, Gibco)
9 supplemented with 10% FBS and 10 mM HEPES (pH 7.5). These images were
10 processed and analyzed with ZEN software. 3D video rendered by using the "3D View"
11 function. Line fluorescence intensities were scanned along arrows and normalized per 3
12 pixels using the "Profile View" function. Line graphs were made by Kyplot software.

13

14 **Aliphatic alcohols treatment on cells**

15 HEK293 cells, which express EGFP, EGFP-afadin, or ZO-1-EGFP, were incubated in
16 DH10 supplemented with 5-10% 1,6-HD (weight/volume, Sigma-Aldrich) for 5 minutes
17 and fixed with 4% PFA at 37°C for 15 minutes. Alternatively, MDCK cells, which were
18 treated with 1 μM LatB for 90 minutes, were incubated in DH10 supplemented with 5%

1,6-HD or 2,5-HD for 5 minutes and then fixed with 4% PFA at 37°C for 15 minutes.

Disassembly of the F-actin polymerization on MDCK cells

Confluent monolayers of afadin KO MDCK cells, which express EGFP-afadin or EGFP-afadinΔC, were incubated in FluoroBrite DMEM supplemented with 1 μM LatB. Live cell imaging was acquired every 3 minutes for a duration of over 180 minutes after LatB addition.

Quantification and statistical analysis

Quantification was represented by the mean ± standard deviation. We performed the Mann-Whitney *U*-test, Steel's multiple comparison test, and Steel and Dwass's multiple comparison test for the non-parametric statistical analyses, as indicated in the figure legends, using Kyplot software. P values of less than 0.05 were regarded as statistically significant.

Data and code availability

All data supporting the current study are available from the corresponding author upon request.

Acknowledgments

The authors are sincerely grateful to Drs. Suzuki, A., Nitta, R., Otani, J., Katsunuma, S., and Ueyama, T. for discussions; Nikon imaging center of Osaka University and Mimori-Kiyosue, Y. for technical assistance. This work was supported by JST PRESTO Grant Number JPMJPR1946 (H.T.); and by JST SPRING Grant Number JPMJSP2148 (S.K.); and by KAKENHI Grants Numbers 19K03634(H.T.), 20H01823(H.T.), and 22K19331(H.T.); and by a grant from the Takeda Science Foundation (H.T.); by Iue Memorial Foundation (S.K.).

The authors declare no conflict of interest.

1 **Abbreviations List**

2 Abbreviations used in this paper: AJ, adherens junction; TJ, tight junction; AJC, apical
3 junctional complex; IDR, intrinsically disordered region; EGFP, enhanced green
4 fluorescent protein; LC, lateral contact; FACS, fluorescence-activated cell sorting; ZA,
5 zonula adherens; h, hours; min, minutes; s, seconds.

6

Figure Legends

Figure 1. Impairment of apical junction formation by loss of afadin

(A) Distribution of afadin (green), α-catenin (red), and F-actin (blue) in WT and afadin-KO cells; apical views of WT or afadin-KO MDCK cells cultured for 24 h and stained for the indicated molecules. Dashed lines indicate the position of vertical section. Arrows indicate scanned regions in the densitometric traces. A representative image is shown of six independent experiments. Scale bars, 10 μm. (X-Z) Vertical sections of the upper images. (Bottom, right) Densitometric traces were performed along the arrows. A.U., arbitrary unit. **(B)** Distribution of α-catenin (green) and β-catenin (magenta) in WT and afadin-KO cells. Merged images are shown; apical views of WT or afadin KO cells cultured for 24 h and stained for α- and β-catenin. Arrowheads indicate the apical cell junctions. Arrows point to the basal edge of the junctions. Scale bars, 10 μm. (X-Z) Vertical sections of the upper images. Scale bars, 10 μm. **(C)** Quantifications of cell height and tilting extent of LCs. Boxes represent mean ± standard deviation (S.D.), and whiskers indicate maximum and minimum values. Tilting extent; n = 30 for WT; n = 30 for afadin KO. Cell height; n = 95 for WT; n = 102 for afadin KO. Mann-Whitney *U*-test; **, $P \leq 0.01$, ***, $P \leq 0.001$. See also figure S2B. **(D)** Distribution of afadin (green), Par-3 (red), and ZO-1 (blue) in WT and afadin-KO cells. WT and afadin KO cells were cultured for 24 h and triple stained with the indicated molecules. Scale bars, 10 μm.

Figure 2. Destabilization of apical junction by lack of C-terminal region of afadin

(A) Distribution of afadins (green), α-catenin (red), and F-actin (blue) in EGFP-afadin

or EGFP-afadinΔC expressing afadin-KO cells. Apical views of the transfectants cultured for 24 h and stained for the indicated molecules. Dashed lines indicate the position of vertical section. Arrows indicate scanned regions in the densitometric traces. A representative image is shown of six independent experiments. Scale bars, 10 μm. (X-Z) Vertical sections of the upper images. (Upper, right) Line scan graphs were performed along the arrows. A.U., arbitrary unit. (Bottom, right) Quantification of tilting extent of LCs. Boxes represent mean ± S.D., and whiskers indicate maximum and minimum values. n = 20 for EGFP-afadin; n = 21 for EGFP-afadinΔC. Mann-Whitney *U*-test; ***, $P \leq 0.001$. **(B)** Cyst formation of the cells expressing EGFP-afadin and EGFP-afadinΔC. These cysts were cultured for 8 days and stained for the indicated molecules. These images show the cross section of the cysts. Arrowheads indicate the apical cell junctions. Arrows point to the lateral contacts of the junctions. Scale bars, 10 μm. **(C)** Distribution of afadins, nectin-1, α-catenin, and F-actin in EGFP-afadin- or EGFP-afadinΔC- and nectin-1-expressing cells. Merged images are shown. Afadin-KO cells stably expressed EGFP-afadin or EGFP-afadinΔC and nectin-1 and were stained with the indicated molecules. Asterisks indicate cells of interest. (Right) Distributions of afadins (green) and exogenous nectin-1 (magenta). Scale bars, 10 μm. (X-Z) Vertical sections of the upper images.

Figure 3. Localization of afadin to the apical junction is due to its self-organizing action

(A) Junction formation of EGFP-afadin and EGFP-afadinΔC-expressing afadin-KO cells. (Left) Apical views of the transfectants cultured for 24 h. Scale bars, 50 μm.

(Right) Time-lapse images of the junction formation; these cells were observed for 250 min at 50 min intervals (See also Video S1&S2). Scale bars, 10 μm. (Bottom) Vertical sections of the upper images. Scale bars, 10 μm. **(B)** Junction formation of nectin-1 and EGFP-afadin- or EGFP-afadinΔC-expressing cells. The signals for EGFP-afadin or EGFP-afadinΔC are shown. (Left) Apical views of the transfectants cultured for 24 h. Scale bars, 50 μm. (Right) Time-lapse images of the junction formation; these cells were observed for 250 min at 50 min intervals (See also Video S3&S4). Scale bars, 10 μm. (Bottom) Vertical sections of the upper images. Scale bars, 10 μm. **(C)** Distribution of afadin (green), ZO-1 (red), and β-catenin (blue) in EGFP-afadin- or EGFP-afadinΔC-expressing cells upon the treatment of Y-27632. Apical views of the transfectants treated with DMSO or 10 μM Y-27632 for 24 h. A representative image is shown of six independent experiments. Scale bars, 10 μm.

Figure 4. C-terminal region of afadin is implicated in condensates formation

(A) Transient expression of EGFP-afadin, EGFP-afadinΔRA, EGFP-afadinΔPDZ, EGFP-afadinΔPR1-2, EGFP-afadinΔCC, EGFP-s-afadin, EGFP-AF_N-PDZ, and EGFP-afadinΔC in HEK293 cells; apical views of the transfectants cultured for 3 days. Dotted lines represent the cell of interest. Arrowheads indicate condensates. Scale bars, 5 μm. (Right) Quantification of EGFP condensate number in the cells. Whiskers represent the mean ± S.D. n = 10 for EGFP-afadin; n = 12 for EGFP-afadinΔRA; n = 12 for EGFP-afadinΔPDZ; n = 15 for EGFP-afadinΔPR1-2; n = 13 for EGFP-afadinΔCC; n = 21 for EGFP-s-afadin; n = 10 for EGFP-AF_N-PDZ; n = 11 for EGFP-afadinΔC. Steel's multiple comparison test; N.S., not significant; ***, $P \leq 0.001$. **(B)** Transient

expression and distribution of EGFP, EGFP-afadin, or ZO-1-EGFP in HEK293 cells in the presence of 1,6-HD; apical views of the transfectants cultured for 3 days. Cells were treated with 1,6-HD for 5 min at 37°C. Dotted lines represent the cell of interest. Arrowheads indicate condensates. Scale bars, 5 μm. (Right) Quantification of condensate number in the cells. Boxes represent mean ± S.D., and whiskers indicate maximum and minimum values. n = 36 for EGFP without 1,6-HD; n = 38 for EGFP with 5% 1.6-HD; n = 41 for EGFP with 10% 1.6-HD; n = 24 for EGFP-afadin without 1,6-HD; n = 43 for EGFP-afadin with 5% 1.6-HD; n = 23 for EGFP-afadin with 10% 1.6-HD; n = 30 for ZO-1-EGFP without 1,6-HD; n = 30 for ZO-1-EGFP with 5% 1,6-HD; n = 29 for ZO-1-EGFP with 10% 1,6-HD. Steel's multiple comparison test; ***, $P \leq 0.001$; N.S., not significant. **(C)** Transient expression of EGFP or EGFP-AF_1114-1654 in HEK293 cells; apical views of the transfectants cultured for 3 days. Dotted lines represent the cell of interest. Arrowheads indicate condensates. Scale bars, 5 μm. (Right) Quantification of EGFP condensate number of the cells. n = 18 for EGFP; n = 12 for EGFP-AF_1114-1654. Mann–Whitney *U*-test; ***, $P \leq 0.001$.

Figure 5. Junctional afadin demonstrates behavior similar to liquid-like condensates

(A) Junction fragmentation in EGFP-afadin, EGFP-afadinΔC, and αE-catenin-EGFP expressing cells by treatment with LatB. (Upper) Apical views of the transfectants before treatment. (Bottom) Apical views of the transfectants after 1 μM LatB treatment for 90 min. Arrowheads and arrows indicate the location of identical junctions before and after treatments. Scale bars, 20 μm. **(B)** Live-cell imaging of junction fragmentation in EGFP-

afadin or EGFP-afadinΔC expressing cells by the treatment of LatB. These cells were observed for 180 min at 15 min interval in the presence of 1 μM LatB. The look-up table represents the intensity of the EGFP signal. Scale bars, 2 μm. Arrowheads indicate condensates. See also Video S13&S14. **(C)** Distribution of afadins in EGFP-afadin- or mScarlet-afadin-expressing afadin-KO MDCK cells upon treatment with LatB. Two transfectants were co-cultured for 3 days and treated with 1 μM LatB for 90 min. The cells were counterstained with phalloidin. Arrowheads indicate the apical cell-cell junctions. Arrows indicate fused condensates between adjacent cells. Scale bars, 2 μm. **(D)** (Left) Distribution of afadin (green) and ZO-1 (magenta) in confluent monolayers of WT MDCK cells upon treatment with LatB and stained for the indicated molecules; apical views of the transfectants treated with 1 μM LatB for 90 min. (Right) Cropped images indicate left images onto dotted squares. Arrowheads and arrows indicate afadin and ZO-1 condensates, respectively. Scale bars, 5 μm. **(E)** Distribution of afadin (green), ZO-1 (red), and α-catenin (blue) of WT MDCK cells upon treatment with 1,6-HD; apical views of the transfectants treated with DMSO or 5% 1,6-HD for 5 min at 37°C and stained for the indicated molecules. Arrowheads indicate the apical cell junctions. A representative image is shown of six independent experiments. Scale bars, 10 μm.

Figure 6. Different IDRs of afadin alter localization within AJC

(A) Localizations of EGFP-afadin-, EGFP-afadinΔC-, or EGFP-afadinΔC+FUSn-expressing afadin-KO cells; apical views of the transfectants cultured for 24 h. Scale bars = 10 μm. **(B)** Close up views of the junctional distribution of afadins (green), ZO-1 (magenta), and β-catenin (grayscale) in EGFP-afadin-, EGFP-afadinΔC+FUSn-, or

EGFP-afadinΔC+PSG-expressing afadin-KO cells; apical views of the transfectants cultured for 24 h and stained with the indicated molecules. Dashed lines indicate the position of vertical section. (X-Z) Vertical sections of the projection images. Scale bars = 1 μm. **(C)** Quantification of peak distance and merged region between afadins and ZO-1 or α-catenin in EGFP-afadin-, EGFP-afadinΔC+FUSn-, or EGFP-afadinΔC+PSG-expressing afadin-KO cells. Whiskers represent the mean ± S.D. Peak distance between afadins and ZO-1; n = 10 for EGFP-afadin, n = 10 for EGFP-afadinΔC+FUSn, n = 10 for EGFP-afadinΔC+PSG. Merged region with afadins and ZO-1; n = 10 for EGFP-afadin, n = 10 for EGFP-afadinΔC+FUSn, n = 10 for EGFP-afadinΔC+PSG. Peak distance between afadins and α-catenin; n = 10 for EGFP -afadin, n = 10 for EGFP-afadinΔC+FUSn, n = 10 for EGFP-afadinΔC+PSG. Merged region with afadins and α-catenin; n = 10 for EGFP-afadin, n = 10 for EGFP-afadinΔC+FUSn, n = 10 for EGFP-afadinΔC+PSG. Steel's multiple comparison test; *, $P \leq 0.05$; **, $P \leq 0.01$; N.S., not significant. **(D)** Schemas of junctional structures of Afadin-KO cells and EGFP-afadin-, EGFP-afadinΔC-, and EGFP-afadinΔC+FUSn-expressing afadin-KO cells.

1 **Supplemental information**

2

3 **Figure S1. Characterization of afadin KO, ZO-1/2 dKO, and αE-catenin KO**

4 **MDCK cells, related to figure 1.**

5 **(A)** Schematic diagram of different afadin fragments. Afadin fragments were tagged

6 with EGFP at the N-terminus. RA, Ras-associated domain; FHA, forkhead-associated

7 domain; DIL, dilute domain; PDZ, PSD95-DLG1-ZO-1 domain; PR, proline-rich

8 region; CC, coiled-coil domain; FAB, F-actin binding domain. +, positive for the

9 interaction with ZO-1, α-catenin, F-actin, or nectins; -, negative for the interaction with

10 ZO-1, α-catenin, F-actin, or nectins. **(B)** Expression levels of afadin and α-tubulin in

11 WT and afadin-KO cells. Cell extracts of WT and KO cells were separated by SDS-

12 PAGE and subjected to western blotting using the indicated Abs. α-tubulin was

13 immunoblotted as a loading control. IB, immunoblot. **(C)** Expression levels of EGFP-

14 afadin and EGFP-afadinΔC in afadin-KO cells. The lowest expressing clones were

15 collected by FACS. **(D)** Distribution of EGFP-afadin, EGFP-afadinΔRA, EGFP-

16 afadinΔPDZ, EGFP-afadinΔPR1-2, EGFP-afadinΔCC, EGFP-s-afadin, EGFP-AF_N-

17 PDZ, and EGFP-afadinΔC in afadin KO cells. The lowest expressing cells were observed

18 by confocal microscopy. A representative image is shown of six independent

experiments. Scale bars = 20 μm. **(E)** Co-immunoprecipitation of ZO-1-HA with the EGFP-afadins. Cell extracts of HEK293 cells transfected with various combinations of the indicated vectors were immunoprecipitated with the anti-GFP Ab. Immunoprecipitates and cell extracts were subjected to western blotting using the anti-afadin and anti-HA Abs. IP, immunoprecipitation. **(F)** Co-immunoprecipitation of α-catenin with the EGFP-afadins. Cell extracts of HEK293 cells transfected with various combinations of the indicated vectors were immunoprecipitated with the anti-GFP. Immunoprecipitates and cell extracts were subjected to western blotting using the anti-afadin and anti-α-catenin Abs. **(G)** Expression levels of ZO-1 and α-tubulin in WT and ZO-1/2 dKO cells. **(H)** Expression levels of α-catenin and α-tubulin in WT and αE-catenin KO cells.

Figure S2. Localizations of afadin mutants upon expression in afadin KO, ZO-1/2 KO, or αE-catenin KO cells, related to figure 2.

(A) Quantifications of cell height of cyst in afadin-KO cells. Whiskers represent mean ± S.D. Cyst height; n = 23 for EGFP-afadin; n = 23 for EGFP-afadinΔC. Mann-Whitney *U*-test; ***, P ≤ 0.001. See also Figure 2B. **(B)** Distribution of endogenous afadin or EGFP-afadinΔC+CC (green), α-catenin (red), and F-actin (blue) in afadin-KO cells or

EGFP-afadinΔC+CC-expressing afadin-KO cells; apical views of the transfectants cultured for 24 h and stained for the indicated molecules. Scale bars, 10 μm. Representative images are shown of six independent experiments. **(C)** Quantifications of tilting extent of LCs in afadin-KO cells. Whiskers represent mean ± S.D. Datasets for EGFP-afadin and EGFP-afadinΔC were equal to those in Figure 1C. Tilting extent; n = 20 for EGFP-afadin; n = 21 for EGFP-afadinΔC; n = 11 for EGFP-afadinΔPR1-2; n = 11 for EGFP-afadinΔCC; n = 20 for EGFP-afadinΔC+CC. Steel and Dwass's multiple comparison test; $P \leq 0.001$; N.S., not significant. **(D)** Distribution of afadin (green), ZO-1 (red), and α-catenin (blue) in ZO-1/2 dKO cells; apical views of ZO-1/2 dKO cells cultured for 24 h and stained for the indicated molecules. Dashed lines indicate the position of vertical section. A representative image is shown of six independent experiments. Scale bars, 10 μm. (Right) Vertical sections of the left images. Arrows indicate the AJCs. Scale bars, 10 μm. **(E)** Distribution of afadin (green), ZO-1 (red), and α-catenin (blue) in αE-catenin KO cells; apical views of αE-catenin KO cells cultured for 24 h and stained for the indicated molecules. Dashed lines indicate the position of vertical sections. Representative images are shown of six independent experiments. Scale bars, 10 μm. (Right) Vertical sections of the left images. Arrows indicate the AJCs. Scale bars, 10 μm.

1

2 **Figure S3. Junctional dynamics of afadin mutants upon expression in afadin KO,**

3 **ZO-1/2 KO, or αE-catenin KO cells, related to figure 3.**

4 **(A)** Junction formation of EGFP-afadinΔPR1-2-, EGFP-afadinΔCC-, and EGFP-

5 afadinΔC+CC-expressing afadin-KO cells. (Left) Apical views of the transfectant of the

6 cells cultured for 24 h. Scale bars, 50 μm. (Right) Time-lapse images of the junction

7 formation in cells observed for 250 min at 50 min intervals. See also Video S5&S6&S7.

8 Scale bars, 10 μm. (Bottom) Vertical sections of the upper images. Scale bars, 10 μm.

9 **(B)** Junction formation of EGFP-afadin- and EGFP-afadinΔC-expressing ZO-1/2-dKO

10 cells. (Left) Apical views of the transfectant. These cells were cultured for 24 h. Scale

11 bars, 50 μm. (Right) Time-lapse images of the junction formation. These cells were

12 observed for 250 min at 50 min intervals. See also Video S8&S9. Scale bars, 10 μm.

13 (Bottom) Vertical sections of the upper images. Scale bars, 10 μm. **(C)** Junction

14 formation of EGFP-afadin- and EGFP-afadinΔC-expressing αE-catenin-KO cells.

15 (Left) Apical views of the transfectant. These cells were cultured for 24 h. Scale bars,

16 50 μm. (Right) Time-lapse images of the junction formation. These cells were observed

17 for 250 min at 50 min intervals. See also Video S10&11. Scale bars, 10 μm. (Bottom)

18 Vertical sections of the upper images. Scale bars, 10 μm.

1

2 **Figure S4. Schematic diagram of afadin IDR mutants and the localization of afadin**

3 **IDR fragments, related to figure 4.**

4 **(A)** Molecular structures of afadin mutants. These afadin fragments were tagged with

5 EGFP at the N-terminus. Predicted IDRs are identified using MobiDB (Piovesan et al.,

6 2018). F-actin-binding (FAB) region was referenced in a previous report (Mandai et al.,

7 1997). +, positive for the interaction with F-actin; -, negative for the interaction with F-

8 actin. **(B)** Fusion of afadin condensates in EGFP-afadin transiently expressing HEK293

9 cells. Apical views of condensates were observed for 2 min at 1 min intervals. Scale bar,

10 1 μm. The look-up table represents the intensity of EGFP signal. Arrowheads indicate

11 points of fusion. m., minutes. A.U., arbitrary unit. See also Video S12. **(C)** Transient

12 expression of EGFP-afadin or EGFP-afadinΔC in ZO-1/2 dKO MDCK cells; apical

13 views of the transfectants cultured for 3 days. Dotted lines represent the cell of interest.

14 Arrowheads indicate condensates. Scale bars, 5 μm. (Right) Quantification of EGFP

15 condensate number of the cells. n = 13 for EGFP; n = 23 for EGFP-afadin. Boxes

16 represent mean ± S.D., and whiskers indicate maximum and minimum values. Mann-

17 Whitney *U*-test; ***, $P \leq 0.001$. **(D)** Localization of the afadin fragments and F-actin in

18 EGFP-AF_1114-1654 or EGFP-AF_C expressing afadin KO cells. Apical views of the

transfectants cultured for 24 h and stained with phalloidin. A representative image is shown of six independent experiments. Scale bars = 10 μm.

Figure S5. Induction of junctional condensate formation, related to figure 5.

(A) Schematic diagram of AJ disruption using experimental F-actin depolymerization. To inactivate the subcellular interactions through F-actin in the AJC, we treated confluent EGFP-afadin- or EGFP-afadinΔC-expressing afadin-KO cells with LatB (Beutel et al., 2019; Kinoshita et al., 2022; Schwayer et al., 2019). **(B)** Distribution of afadin in confluent monolayers of WT MDCK cells by the sequential treatment of LatB and aliphatic alcohols. These cells were treated with 1 μM LatB for 90 min at 37°C. Subsequently, these cells were treated with 5% 1,6-HD or 2,5-HD for 5 min at 37°C and stained for the endogenous afadin. Arrowheads indicate condensates. A representative image is shown of six independent experiments. Scale bars, 10 μm.

Figure S6. Molecular structures of afadin chimeras, related to figure 6.

(A) Schematic of the reconstructed afadin chimeras. The afadin chimeras were tagged with EGFP at the N-terminus. FUSn is the N-terminal IDR of the RNA-binding protein Fused in Sarcoma (FUS) (Burke et al., 2015; Shin et al., 2017). ZO-1_PSG requires

dimerization of ZO-1 and recruitment of AJ (Shimobayashi et al., 2021; Umeda et al., 2006). **(B)** Transient expression of EGFP-afadin, EGFP-afadinΔC, EGFP-afadinΔC+FUSn, or EGFP-afadinΔC+PSG in HEK293 cells; apical views of the transfectants cultured for 3 days. Dotted lines represent the cell of interest. Arrowheads indicate condensates. Scale bars, 5 μm. (Bottom) Quantification of EGFP condensate number in the cells. Whiskers represent the mean ± S.D. n = 9 for EGFP-afadin; n = 28 for EGFP-afadinΔC; n = 19 for EGFP-afadinΔC+FUSn; n = 13 for EGFP-afadinΔC+PSG. Steel and Dwass's multiple comparison test; ***, $P \leq 0.001$.

Video legends

Video S1 Junction formation of EGFP-afadin expressing cells, related to figure 3.

Apical views of the transfectants. Cells were cultured for 24 h. Time-lapse images of the junction formation. Cells were observed for 250 min at 10 min intervals. Scale bars, 10 μm.

Video S2 Junction formation of EGFP-afadinΔC expressing afadin KO cells, related to figure 3.

Apical views of the transfectants. Cells were cultured for 24 h. Time-lapse images of the junction formation. Cells were observed for 250 min at 10 min intervals. Scale bars, 10 μm.

Video S3 Junction formation of nectin-1 and EGFP-afadin expressing afadin KO cells, related to figure 3.

Apical views of the transfectants. Cells were cultured for 24 h. Time-lapse images of the junction formation. Cells were observed for 250 min at 10 min intervals. Scale bars, 10 μm.

Video S4 Junction formation of nectin-1 and EGFP-afadinΔC expressing afadin KO cells, related to figure 3.

Apical views of the transfectants. Cells were cultured for 24 h. Time-lapse images of the junction formation. Cells were observed for 250 min at 10 min intervals. Scale bars, 10 μm.

Video S5 Junction formation of EGFP-afadinΔPR1-2 expressing afadin KO cells, related to figure S3.

Apical views of the transfectants. Cells were cultured for 24 h. Time-lapse images of the junction formation. Cells were observed for 250 min at 10 min intervals. Scale bars, 10 μm.

Video S6 Junction formation of EGFP-afadinΔCC expressing afadin KO cells, related to figure S3.

Apical views of the transfectants. Cells were cultured for 24 h. Time-lapse images of the junction formation. Cells were observed for 250 min at 10 min intervals. Scale bars, 10 μm..

Video S7 Junction formation of EGFP-afadinΔC+CC expressing afadin KO cells, related to figure S3.

Apical views of the transfectants. Cells were cultured for 24 h. Time-lapse images of the junction formation. Cells were observed for 250 min at 10 min intervals. Scale bars, 10 μm.

Video S8 Junction formation of EGFP-afadin expressing ZO-1/2 dKO cells, related to figure S3.

Apical views of the transfectants. Cells were cultured for 24 h. Time-lapse images of the junction formation. Cells were observed for 250 min at 10 min intervals. Scale bars, 10 μm.

Video S9 Junction formation of EGFP-afadinΔC expressing ZO-1/2 dKO cells, related to figure S3.

Apical views of the transfectants. Cells were cultured for 24 h. Time-lapse images of the junction formation. Cells were observed for 250 min at 10 min intervals. Scale bars, 10 μm.

Video S10 Junction formation of EGFP-afadin expressing αE-catenin KO cells, related to figure S3.

Apical views of the transfectants. Cells were cultured for 24 h. Time-lapse images of the junction formation. Cells were observed for 250 min at 10 min intervals. Scale bars, 10 μm.

Video S11 Junction formation of EGFP-afadinΔC expressing αE-catenin KO cells, related to figure S3.

Apical views of the transfectants. Cells were cultured for 24 h. Time-lapse images of the junction formation. Cells were observed for 250 min at 10 min intervals. Scale bars, 10 μm.

Video S12 Condensates formation of EGFP-afadin, related to figure 4.

3D views of the transfectants. The cell was transfected transiently after 3 days. This cell was observed for 200 min at 1-min intervals. The upper side of the video shows the apical side of the cell and the lower side shows the basal side. Grid scales indicate per 2 μm.

Video S13 Molecular dynamics of EGFP-afadin by the treatment of LatB, related to figure 5.

Apical views of the transfectants. These confluent cells were observed for 180 min at 3 min intervals in the presence of 1 μM LatB. The look-up table represents the strength of the EGFP signal, with magenta indicating the maximum threshold and black indicating the minimum threshold. Scale bars, 2 μm.

Video S14 Molecular dynamics of EGFP-afadinΔC by the treatment of LatB, related to figure 5.

Apical views of the transfectants. These confluent cells were observed for 180 min at 3 min intervals in the presence of 1 μM LatB. The look-up table represents the strength of the EGFP signal, with magenta indicating the maximum threshold and black indicating the minimum threshold. Scale bars, 2 μm.

Reference

Anderson, J.M., B.R. Stevenson, L.A. Jesaitis, D.A. Goodenough, and M.S. Mooseker. 1988. Characterization of ZO-1, a protein component of the tight junction from mouse liver and Madin-Darby canine kidney cells. *J Cell Biol*. 106:1141-1149.

Beutel, O., R. Maraspini, K. Pombo-Garcia, C. Martin-Lemaitre, and A. Honigmann. 2019. Phase Separation of Zonula Occludens Proteins Drives Formation of Tight Junctions. *Cell*. 179:923-936 e911.

Bindels, D.S., L. Haarbosch, L. van Weeren, M. Postma, K.E. Wiese, M. Mastop, S. Aumonier, G. Gotthard, A. Royant, M.A. Hink, and T.W. Gadella, Jr. 2017. mScarlet: a bright monomeric red fluorescent protein for cellular imaging. *Nat Methods*. 14:53-56.

Blose, S.H., D.I. Meltzer, and J.R. Feramisco. 1984. 10-nm filaments are induced to collapse in living cells microinjected with monoclonal and polyclonal antibodies against tubulin. *J Cell Biol*. 98:847-858.

Bonello, T.T., K.Z. Perez-Vale, K.D. Sumigray, and M. Peifer. 2018. Rap1 acts via multiple mechanisms to position Canoe and adherens junctions and mediate apical-basal polarity establishment. *Development*. 145.

Burke, K.A., A.M. Janke, C.L. Rhine, and N.L. Fawzi. 2015. Residue-by-Residue View of In Vitro FUS Granules that Bind the C-Terminal Domain of RNA Polymerase II. *Mol Cell*. 60:231-241.

Choi, W., B.R. Acharya, G. Peyret, M.A. Fardin, R.M. Mege, B. Ladoux, A.S. Yap, A.S. Fanning, and M. Peifer. 2016. Remodeling the zonula adherens in response to tension and the role of afadin in this response. *J Cell Biol*. 213:243-260.

Drenckhahn, D., and H. Franz. 1986. Identification of actin-, alpha-actinin-, and vinculin-containing plaques at the lateral membrane of epithelial cells. *J Cell Biol*. 102:1843-1852.

Farquhar, M.G., and G.E. Palade. 1963. Junctional complexes in various epithelia. *J Cell Biol*. 17:375-412.

Graham, F.L., J. Smiley, W.C. Russell, and R. Nairn. 1977. Characteristics of a human cell line transformed by DNA from human adenovirus type 5. *J Gen Virol*. 36:59-74.

Gurley, N.J., R.A. Szymanski, R.H. Dowen, T.A. Butcher, N. Ishiyama, and M. Peifer. 2023. Exploring the evolution and function of Canoe's intrinsically disordered region in linking cell-cell junctions to the cytoskeleton during embryonic

morphogenesis. *PLoS One*. 18:e0289224.
Hoshino, T., T. Sakisaka, T. Baba, T. Yamada, T. Kimura, and Y. Takai. 2005. Regulation of E-cadherin endocytosis by nectin through afadin, Rap1, and p120ctn. *J Biol Chem*. 280:24095-24103.
Huxham, J., S. Tabaries, and P.M. Siegel. 2021. Afadin (AF6) in cancer progression: A multidomain scaffold protein with complex and contradictory roles. *Bioessays*. 43:e2000221.
Ichii, T., and M. Takeichi. 2007. p120-catenin regulates microtubule dynamics and cell migration in a cadherin-independent manner. *Genes Cells*. 12:827-839.
Ikeda, W., H. Nakanishi, J. Miyoshi, K. Mandai, H. Ishizaki, M. Tanaka, A. Togawa, K. Takahashi, H. Nishioka, H. Yoshida, A. Mizoguchi, S. Nishikawa, and Y. Takai. 1999. Afadin: A key molecule essential for structural organization of cell-cell junctions of polarized epithelia during embryogenesis. *J Cell Biol*. 146:1117-1132.
Itoh, Y., S. Iida, S. Tamura, R. Nagashima, K. Shiraki, T. Goto, K. Hibino, S. Ide, and K. Maeshima. 2021. 1,6-hexanediol rapidly immobilizes and condenses chromatin in living human cells. *Life Sci Alliance*. 4.
Johnson, K.R., J.E. Lewis, D. Li, J. Wahl, A.P. Soler, K.A. Knudsen, and M.J. Wheelock. 1993. P- and E-cadherin are in separate complexes in cells expressing both cadherins. *Exp Cell Res*. 207:252-260.
Katsunuma, S., H. Honda, T. Shinoda, Y. Ishimoto, T. Miyata, H. Kiyonari, T. Abe, K. Nibu, Y. Takai, and H. Togashi. 2016. Synergistic action of nectins and cadherins generates the mosaic cellular pattern of the olfactory epithelium. *J Cell Biol*. 212:561-575.
Keder, A., N. Rives-Quinto, B.L. Aerne, M. Franco, N. Tapon, and A. Carmena. 2015. The hippo pathway core cassette regulates asymmetric cell division. *Curr Biol*. 25:2739-2750.
Kinoshita, N., T.S. Yamamoto, N. Yasue, C. Takagi, T. Fujimori, and N. Ueno. 2022. Force-dependent remodeling of cytoplasmic ZO-1 condensates contributes to cell-cell adhesion through enhancing tight junctions. *iScience*. 25:103846.
Kobayashi, R., S. Kurita, M. Miyata, T. Maruo, K. Mandai, Y. Rikitake, and Y. Takai. 2014. s-Afadin binds more preferentially to the cell adhesion molecules nectins than l-afadin. *Genes Cells*. 19:853-863.
Komura, H., H. Ogita, W. Ikeda, A. Mizoguchi, J. Miyoshi, and Y. Takai. 2008. Establishment of cell polarity by afadin during the formation of embryoid bodies. *Genes Cells*. 13:79-90.

Lin, Y., E. Mori, M. Kato, S. Xiang, L. Wu, I. Kwon, and S.L. McKnight. 2016. Toxic PR Poly-Dipeptides Encoded by the C9orf72 Repeat Expansion Target LC Domain Polymers. *Cell*. 167:789-802 e712.

Mandai, K., H. Nakanishi, A. Satoh, H. Obaishi, M. Wada, H. Nishioka, M. Itoh, A. Mizoguchi, T. Aoki, T. Fujimoto, Y. Matsuda, S. Tsukita, and Y. Takai. 1997. Afadin: A novel actin filament-binding protein with one PDZ domain localized at cadherin-based cell-to-cell adherens junction. *J Cell Biol*. 139:517-528.

Mandai, K., Y. Rikitake, Y. Shimono, and Y. Takai. 2013. Afadin/AF-6 and canoe: roles in cell adhesion and beyond. *Prog Mol Biol Transl Sci*. 116:433-454.

Mangeol, P., D. Massey-Harroche, M. Sebbagh, F. Richard, A. Le Bivic, and P.F. Lenne. 2024. The zonula adherens matura redefines the apical junction of intestinal epithelia. *Proc Natl Acad Sci U S A*. 121:e2316722121.

Maruo, T., S. Sakakibara, M. Miyata, Y. Itoh, S. Kurita, K. Mandai, T. Sasaki, and Y. Takai. 2018. Involvement of l-afadin, but not s-afadin, in the formation of puncta adherentia junctions of hippocampal synapses. *Mol Cell Neurosci*. 92:40-49.

Matsuda, M., A. Kubo, M. Furuse, and S. Tsukita. 2004. A peculiar internalization of claudins, tight junction-specific adhesion molecules, during the intercellular movement of epithelial cells. *J Cell Sci*. 117:1247-1257.

Nakata, S., N. Fujita, Y. Kitagawa, R. Okamoto, H. Ogita, and Y. Takai. 2007. Regulation of platelet-derived growth factor receptor activation by afadin through SHP-2: implications for cellular morphology. *J Biol Chem*. 282:37815-37825.

Nishimura, T., S. Ito, H. Saito, S. Hiver, K. Shigetomi, J. Ikenouchi, and M. Takeichi. 2016. DAAM1 stabilizes epithelial junctions by restraining WAVE complex-dependent lateral membrane motility. *J Cell Biol*. 215:559-573.

Noordstra, I., M.D. Hermoso, L. Schimmel, A. Bonfim-Melo, D. Currin-Ross, C.N. Duong, J.M. Kalappurakkal, R.G. Morris, D. Vestweber, S. Mayor, E. Gordon, P. Roca-Cusachs, and A.S. Yap. 2023. An E-cadherin-actin clutch translates the mechanical force of cortical flow for cell-cell contact to inhibit epithelial cell locomotion. *Dev Cell*. 58:1748-1763 e1746.

Ooshio, T., R. Kobayashi, W. Ikeda, M. Miyata, Y. Fukumoto, N. Matsuzawa, H. Ogita, and Y. Takai. 2010. Involvement of the interaction of afadin with ZO-1 in the formation of tight junctions in Madin-Darby canine kidney cells. *The Journal of biological chemistry*. 285:5003-5012.

Otani, T., T. Ichii, S. Aono, and M. Takeichi. 2006. Cdc42 GEF Tuba regulates the junctional configuration of simple epithelial cells. *J Cell Biol*. 175:135-146.

Otani, T., T.P. Nguyen, S. Tokuda, K. Sugihara, T. Sugawara, K. Furuse, T. Miura, K.

Ebnet, and M. Furuse. 2019. Claudins and JAM-A coordinately regulate tight junction formation and epithelial polarity. *J Cell Biol*. 218:3372-3396.

Patel, A., H.O. Lee, L. Jawerth, S. Maharana, M. Jahnel, M.Y. Hein, S. Stoynov, J. Mahamid, S. Saha, T.M. Franzmann, A. Pozniakovski, I. Poser, N. Maghelli, L.A. Royer, M. Weigert, E.W. Myers, S. Grill, D. Drechsel, A.A. Hyman, and S. Alberti. 2015. A Liquid-to-Solid Phase Transition of the ALS Protein FUS Accelerated by Disease Mutation. *Cell*. 162:1066-1077.

Piovesan, D., F. Tabaro, L. Paladin, M. Necci, I. Micetic, C. Camilloni, N. Davey, Z. Dosztanyi, B. Meszaros, A.M. Monzon, G. Parisi, E. Schad, P. Sormanni, P. Tompa, M. Vendruscolo, W.F. Vranken, and S.C.E. Tosatto. 2018. MobiDB 3.0: more annotations for intrinsic disorder, conformational diversity and interactions in proteins. *Nucleic Acids Res*. 46:D471-D476.

Richardson, J.C., V. Scalera, and N.L. Simmons. 1981. Identification of two strains of MDCK cells which resemble separate nephron tubule segments. *Biochim Biophys Acta*. 673:26-36.

Rouaud, F., S. Sluysmans, A. Flinois, J. Shah, E. Vasileva, and S. Citi. 2020. Scaffolding proteins of vertebrate apical junctions: structure, functions and biophysics. *Biochim Biophys Acta Biomembr*. 1862:183399.

Sakakibara, S., K. Mizutani, A. Sugiura, A. Sakane, T. Sasaki, S. Yonemura, and Y. Takai. 2020. Afadin regulates actomyosin organization through alphaE-catenin at adherens junctions. *J Cell Biol*. 219.

Sawyer, J.K., N.J. Harris, K.C. Slep, U. Gaul, and M. Peifer. 2009. The Drosophila afadin homologue Canoe regulates linkage of the actin cytoskeleton to adherens junctions during apical constriction. *J Cell Biol*. 186:57-73.

Schwayer, C., S. Shamipour, K. Pranjic-Ferscha, A. Schauer, M. Balda, M. Tada, K. Matter, and C.P. Heisenberg. 2019. Mechanosensation of Tight Junctions Depends on ZO-1 Phase Separation and Flow. *Cell*. 179:937-952 e918.

Shimobayashi, S.F., P. Ronceray, D.W. Sanders, M.P. Haataja, and C.P. Brangwynne. 2021. Nucleation landscape of biomolecular condensates. *Nature*. 599:503-506.

Shin, Y., J. Berry, N. Pannucci, M.P. Haataja, J.E. Toettcher, and C.P. Brangwynne. 2017. Spatiotemporal Control of Intracellular Phase Transitions Using Light-Activated optoDroplets. *Cell*. 168:159-171 e114.

Sun, Y., S.Y. Lau, Z.W. Lim, S.C. Chang, F. Ghadessy, A. Partridge, and A. Miserez. 2022. Phase-separating peptides for direct cytosolic delivery and redox-activated release of macromolecular therapeutics. *Nat Chem*. 14:274-283.

Tachibana, K., H. Nakanishi, K. Mandai, K. Ozaki, W. Ikeda, Y. Yamamoto, A.

Nagafuchi, S. Tsukita, and Y. Takai. 2000. Two cell adhesion molecules, nectin and cadherin, interact through their cytoplasmic domain-associated proteins. *J Cell Biol*. 150:1161-1176.

Takahashi, K., H. Nakanishi, M. Miyahara, K. Mandai, K. Satoh, A. Satoh, H. Nishioka, J. Aoki, A. Nomoto, A. Mizoguchi, and Y. Takai. 1999. Nectin/PRR: an immunoglobulin-like cell adhesion molecule recruited to cadherin-based adherens junctions through interaction with Afadin, a PDZ domain-containing protein. *J Cell Biol*. 145:539-549.

Takai, Y., W. Ikeda, H. Ogita, and Y. Rikitake. 2008. The immunoglobulin-like cell adhesion molecule nectin and its associated protein afadin. *Annu Rev Cell Dev Biol*. 24:309-342.

Takai, Y., and H. Nakanishi. 2003. Nectin and afadin: novel organizers of intercellular junctions. *J Cell Sci*. 116:17-27.

Takeichi, M. 2014. Dynamic contacts: rearranging adherens junctions to drive epithelial remodelling. *Nat Rev Mol Cell Biol*. 15:397-410.

Togashi, H., K. Kominami, M. Waseda, H. Komura, J. Miyoshi, M. Takeichi, and Y. Takai. 2011. Nectins Establish a Checkerboard-like Cellular Pattern in the Auditory Epithelium. *Science*. 333:1144-1147.

Uehata, M., T. Ishizaki, H. Satoh, T. Ono, T. Kawahara, T. Morishita, H. Tamakawa, K. Yamagami, J. Inui, M. Maekawa, and S. Narumiya. 1997. Calcium sensitization of smooth muscle mediated by a Rho-associated protein kinase in hypertension. *Nature*. 389:990-994.

Umeda, K., J. Ikenouchi, S. Katahira-Tayama, K. Furuse, H. Sasaki, M. Nakayama, T. Matsui, S. Tsukita, and M. Furuse. 2006. ZO-1 and ZO-2 independently determine where claudins are polymerized in tight-junction strand formation. *Cell*. 126:741-754.

Vogelmann, R., and W.J. Nelson. 2005. Fractionation of the epithelial apical junctional complex: reassessment of protein distributions in different substructures. *Mol Biol Cell*. 16:701-716.

Wee, B., C.A. Johnston, K.E. Prehoda, and C.Q. Doe. 2011. Canoe binds RanGTP to promote Pins(TPR)/Mud-mediated spindle orientation. *J Cell Biol*. 195:369-376.

Yang, Z., S. Zimmerman, P.R. Brakeman, G.M. Beaudoin, L.F. Reichardt, and D.K. Marciano. 2013. De novo lumen formation and elongation in the developing nephron: a central role for afadin in apical polarity. *Development*. 140:1774-1784.

Yoshioka, K. 2002. KyPlot as a Tool for Graphical Data Analysis. Physica-Verlag HD. 37-46.

Zhadanov, A.B., D.W. Provance, Jr., C.A. Speer, J.D. Coffin, D. Goss, J.A. Blixt, C.M. Reichert, and J.A. Mercer. 1999. Absence of the tight junctional protein AF-6 disrupts epithelial cell-cell junctions and cell polarity during mouse development. *Curr Biol*. 9:880-888.

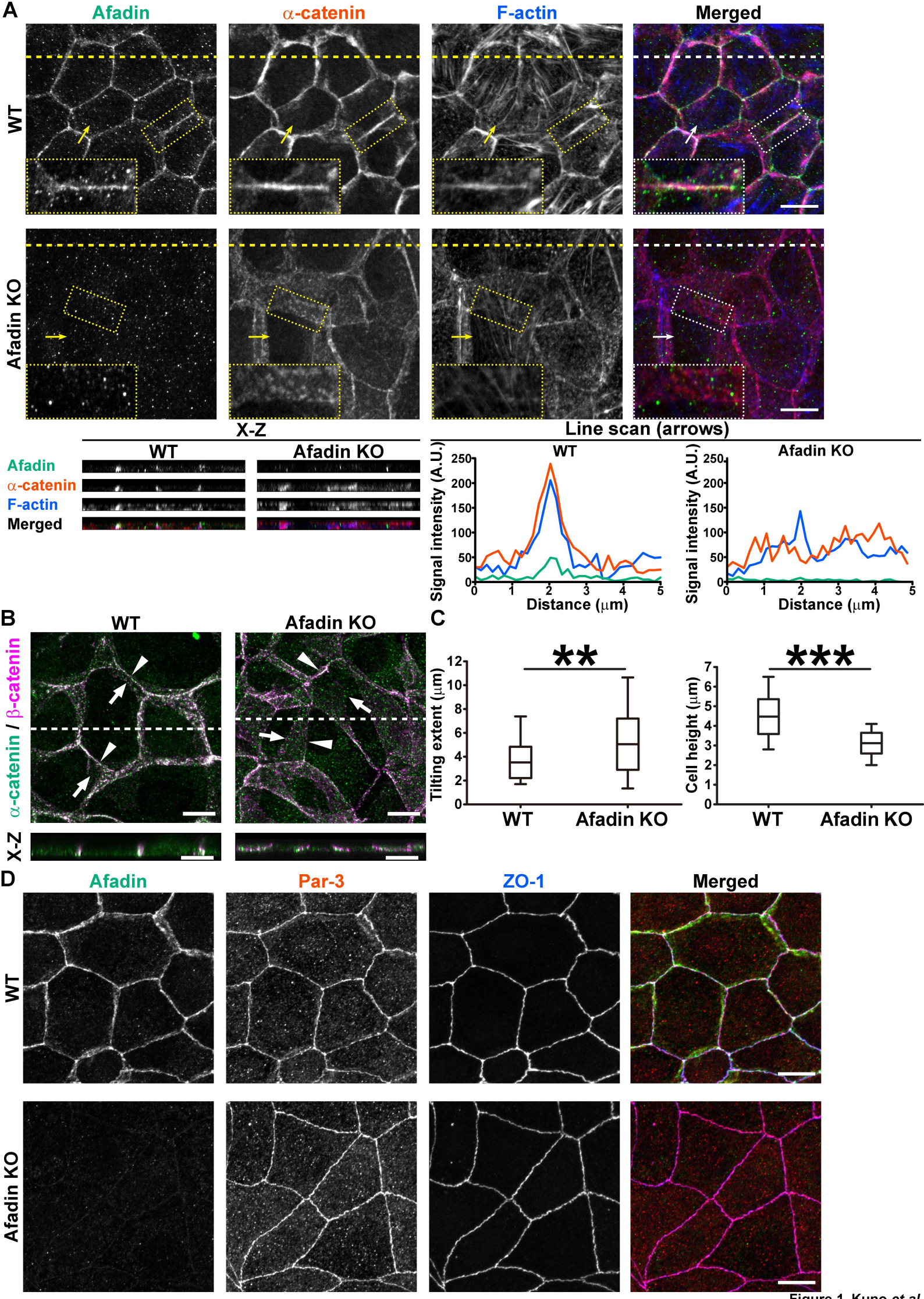

Figure 1 Kuno *et al.*

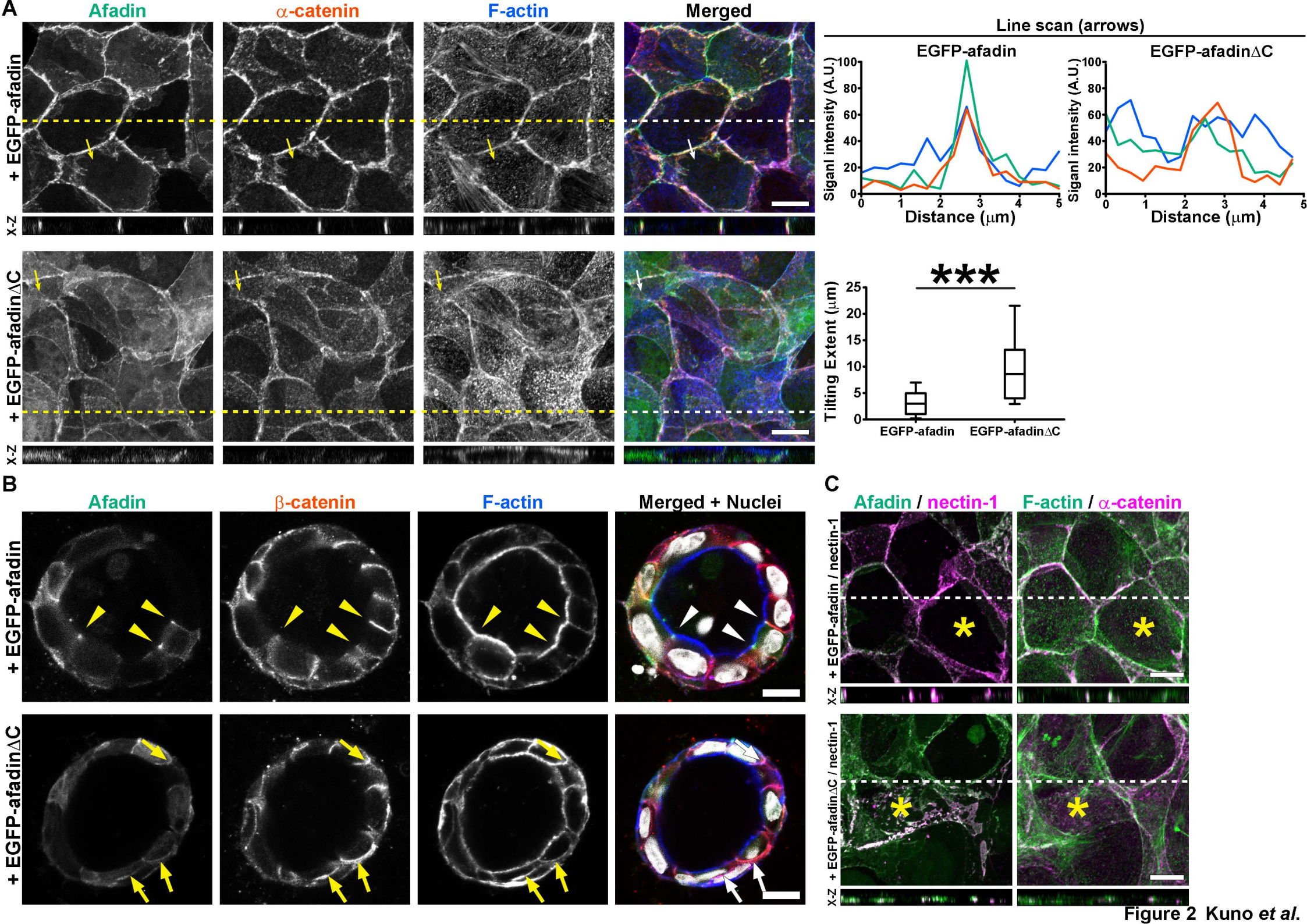

Figure 2 Kuno *et al.*

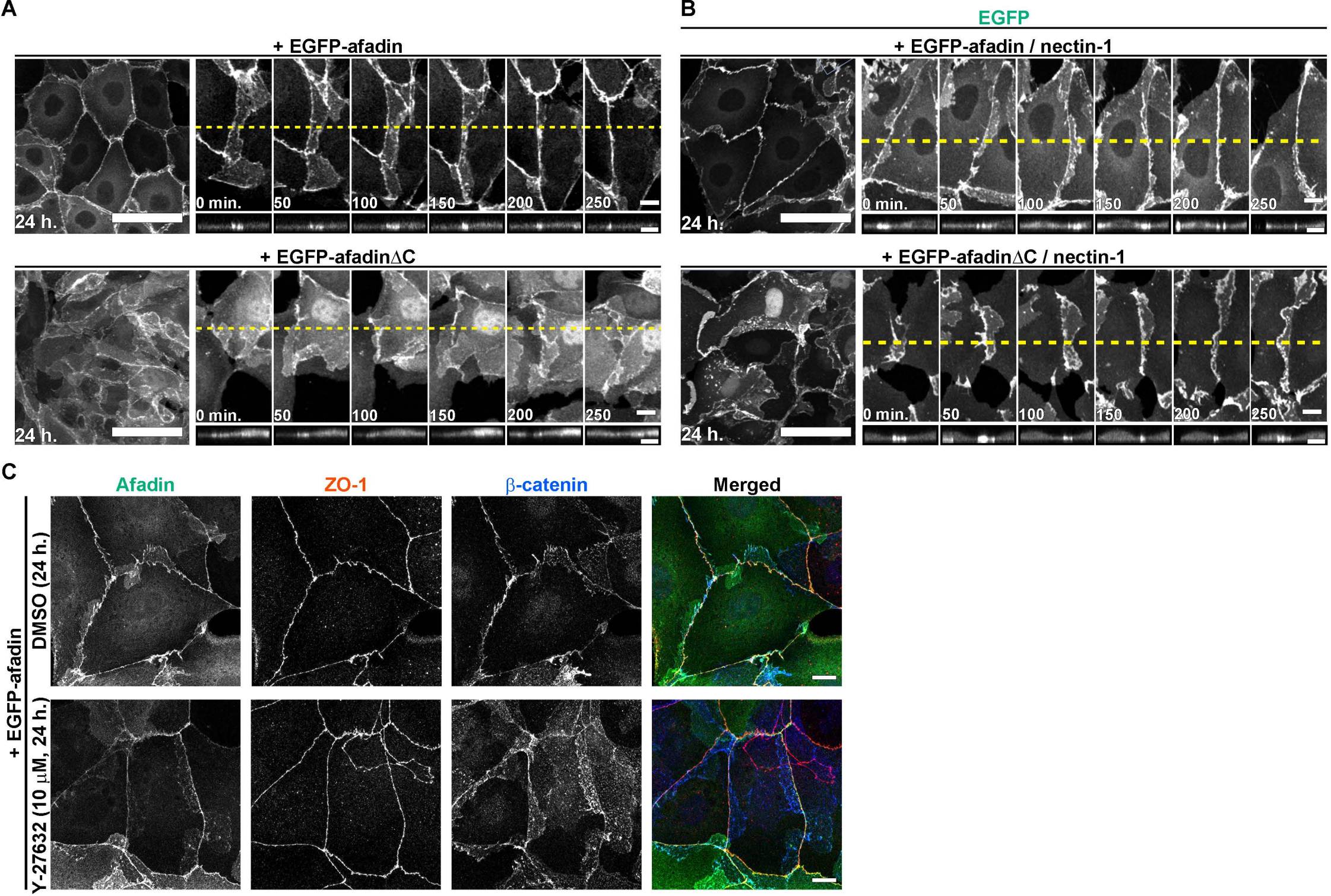

Figure 3 Kuno *et al.*

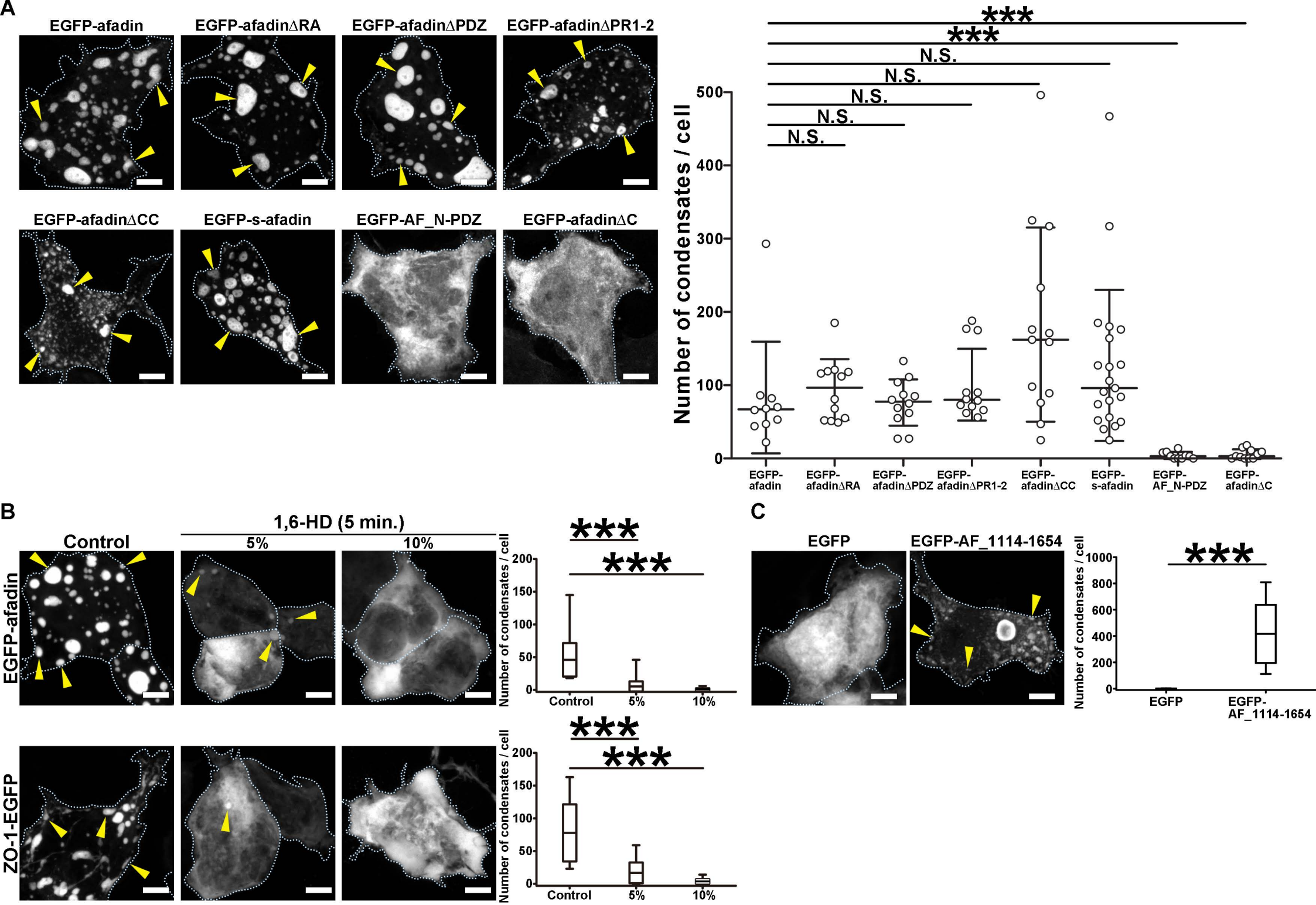

Figure 4 Kuno *et al.*

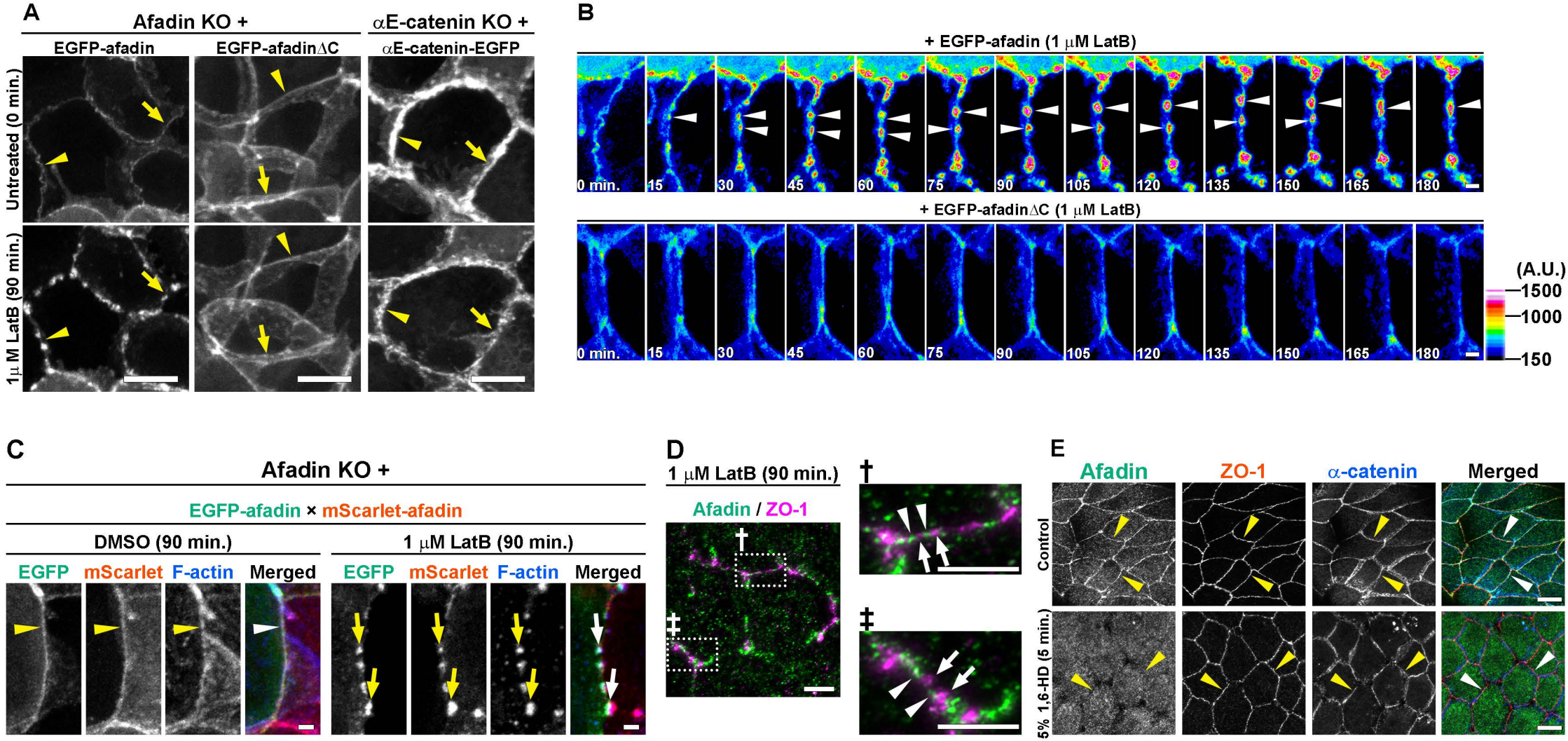

Figure 5 Kuno *et al.*

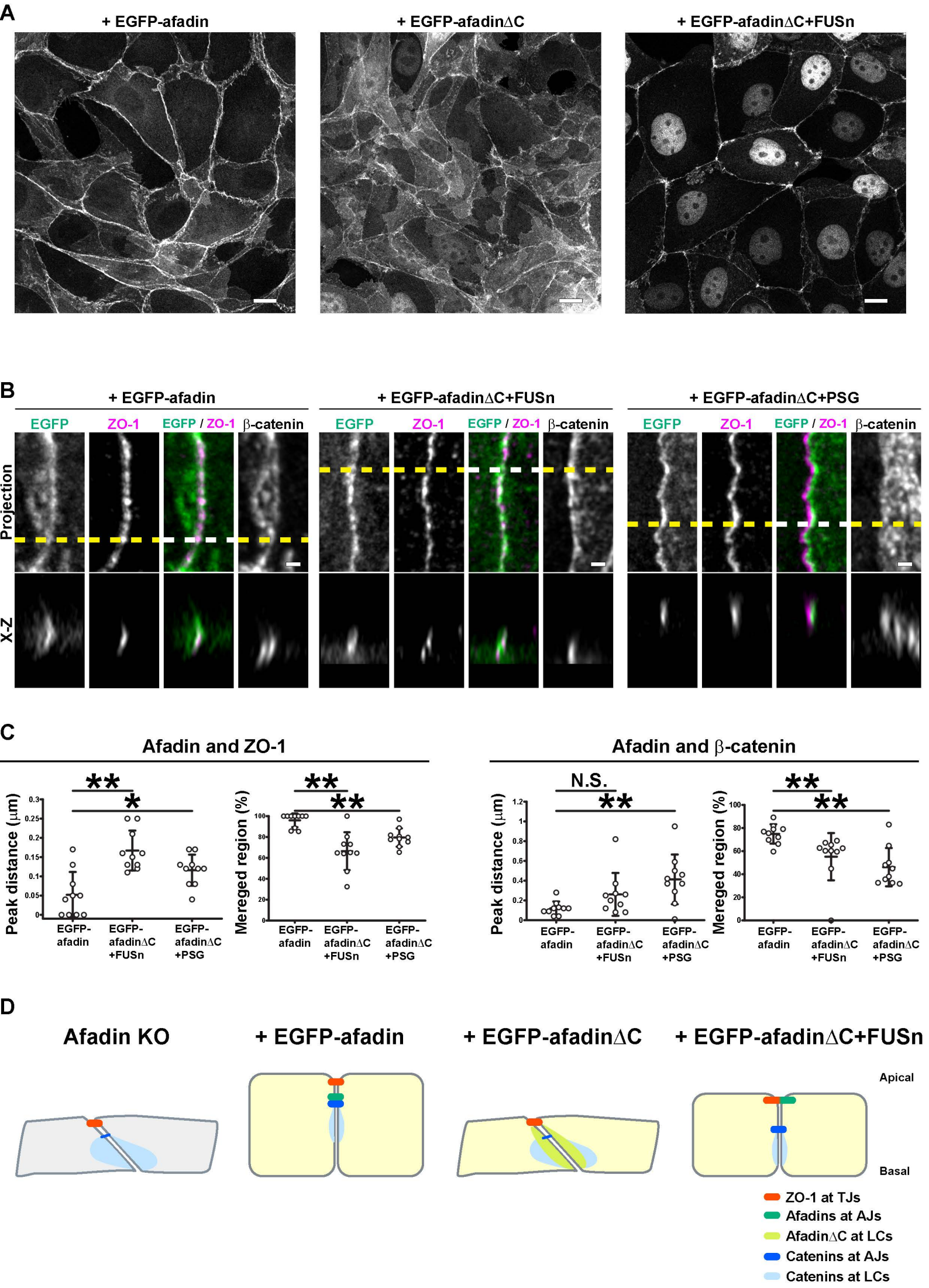

Figure 6 Kuno *et al.*